Journal of General Virology

# FIG4 is a Hepatitis C Virus particle-bound protein implicated in virion morphogenesis and infectivity with cholesteryl esters modulation potential

--Manuscript Draft--

| | |
|---|---|
| **Manuscript Number:** | VIR-D-15-00316R1 |
| **Full Title:** | FIG4 is a Hepatitis C Virus particle-bound protein implicated in virion morphogenesis and infectivity with cholesteryl esters modulation potential |
| **Short Title:** | FIG4 and HCV |
| **Article Type:** | Standard |
| **Section/Category:** | Animal - Positive-strand RNA Viruses |
| **Corresponding Author:** | Romain Parent<br>CRCL University of Lyon<br>FRANCE |
| **First Author:** | Jessica Cottarel |
| **Order of Authors:** | Jessica Cottarel |
| | Marie-Laure Plissonnier |
| | Majlinda Kullolli |
| | Sharon Pitteri |
| | Sophie Clément |
| | Valentina Millarte |
| | Si-Nafa Si-Ahmed |
| | Hesso Farhan |
| | Fabien Zoulim |
| | Romain Parent |
| **Abstract:** | There is growing evidence that virus particles also contain host cell proteins, which provide viruses with certain properties required for entry and release. A proteomic analysis performed on double gradient-purified hepatitis C virus from two highly viremic patients identified the Phosphatidylinositol 3,5-bisphosphate 5-phosphatase FIG4 (KIAA0274) as part of the viral particles. We validated the association using immunoelectron microscopy, immunoprecipitation and neutralization assays in vitro as well as patient-derived virus particles. RNAi-mediated reduction of FIG4 expression decreased cholesteryl ester (CE) levels along with intra- and extracellular viral infectivity without affecting HCV RNA levels. Likewise, overexpressing FIG4 increased intracellular CE levels as well as intra- and extracellular viral infectivity without affecting viral RNA levels. Triglyceride (TG) levels and lipid droplets (LD) parameters remained unaffected. The 3,5-bisphosphate 5-phosphatase active site of FIG4 was found to strongly condition these results. While FIG4 was found to localize to areas corresponding to viral assembly sites, at the immediate vicinity of LDs in calnexin+ and HCV core+ regions, no implication of FIG4 in the secretory pathway of the hepatocytes could be found using either FIG4 null mice, in vitro morphometry or functional assays of the ERGIC/Golgi compartments. This indicates that FIG4-dependent modulation of HCV infectivity is unrelated to alterations in the functionality of the secretory pathway. Because of the documented implication of CE in the composition and infectivity of HCV particles, these results suggest that FIG4 binds to HCV and modulates particle formation in a CE-related manner. |

response to rev.
Click here to download Response to Reviewer: Response to the reviewers.docx

# FIG4 is a Hepatitis C Virus particle-bound protein implicated in virion morphogenesis and infectivity with cholesteryl esters modulation potential

**Running title: FIG4 and HCV**

**Category**: Positive strand RNA viruses; regular article

**Authors:**

Jessica Cottarel[1], Marie-Laure Plissonnier[1], Majlinda Kullolli[2], Sharon Pitteri[2], Sophie Clément[3], Valentina Millarte[4], Si-Nafa Si-Ahmed[5], Hesso Farhan[4], Fabien Zoulim[1,5], Romain Parent[1*].

**Affiliations:**

[1] Pathogenesis of Hepatitis B and C - DEVweCAN LabEx, INSERM U1052-CNRS 5286, Centre de Recherche en Cancérologie de Lyon, Université de Lyon, F-69008 Lyon, France

[2] Canary Center for Cancer Early Detection, Department of Radiology, Stanford University School of Medicine, Palo Alto, CA 94304

[3] Department of Clinical Pathology, University of Geneva, Geneva, Switzerland

[4] Department of Biology, University of Konstanz, Germany; Biotechnology Institute Thurgau, Kreuzlingen, Switzerland

[5] Hospices Civils de Lyon, Service d'Hépatogastroentérologie, F-69001 Lyon, France

**Corresponding author:** Romain Parent, E-mail: romain.parent@inserm.fr, Phone: +00 33 4 72 68 19 70, Fax: +00 33 4 72 68 19 71. Mailing address: Inserm U1052, 151 Cours Albert Thomas, F-69424 Lyon Cedex 03, France.

**Conflict of interest statement:** None

**Word count**: 240 (summary); 5056 (main text)
**Number of figures**: 8
**Number of Supplementary figures**: 9
**Number of Supplementary tables**: 1

**Abstract**

There is growing evidence that virus particles also contain host cell proteins, which provide viruses with certain properties required for entry and release. A proteomic analysis performed on double gradient-purified hepatitis C virus from two highly viremic patients identified the Phosphatidylinositol 3,5-bisphosphate 5-phosphatase FIG4 (KIAA0274) as part of the viral particles. We validated the association using immunoelectron microscopy, immunoprecipitation and neutralization assays in vitro as well as patient-derived virus particles. RNAi-mediated reduction of FIG4 expression decreased cholesteryl ester (CE) levels along with intra- and extracellular viral infectivity without affecting HCV RNA levels. Likewise, overexpressing FIG4 increased intracellular CE levels as well as intra- and extracellular viral infectivity without affecting viral RNA levels. Triglyceride (TG) levels and lipid droplets (LD) parameters remained unaffected. The 3,5-bisphosphate 5-phosphatase active site of FIG4 was found to strongly condition these results. While FIG4 was found to localize to areas corresponding to viral assembly sites, at the immediate vicinity of LDs in calnexin+ and HCV core+ regions, no implication of FIG4 in the secretory pathway of the hepatocytes could be found using either FIG4 null mice, in vitro morphometry or functional assays of the ERGIC/Golgi compartments. This indicates that FIG4-dependent modulation of HCV infectivity is unrelated to alterations in the functionality of the secretory pathway. Because of the documented implication of CE in the composition and infectivity of HCV particles, these results suggest that FIG4 binds to HCV and modulates particle formation in a CE-related manner.

## Introduction

The hepatitis C virus (HCV) is a small enveloped positive-strand RNA strand virus and belongs to the genus *Hepacivirus* in the *Flaviviridae* family. A hallmark of HCV is its high propensity to establish persistent infection in humans, which in many cases leads to chronic liver disease, cirrhosis, and hepatocellular carcinoma (El-Serag, 2012).

HCV infects hepatocytes and stimulates the accumulation of cholesteryl esters (CE) preferentially in cytoplasmic lipid droplets (LDs). The virus also induces extensive remodeling of endoplasmic reticulum (ER)-derived membranes into a so-called "membranous web" (Egger *et al.*, 2002). This web is composed of chosterol-rich double membrane vesicles located in close proximity to LDs and serve as site of viral genome replication and particle assembly (Aizaki *et al.*, 2004; Bartenschlager *et al.*, 2011; Paul *et al.*, 2013). HCV possesses a single RNA molecule which is first translated into a large polyprotein of roughly 3,000 amino acids and then co- and posttranslationally processed into the individual viral proteins by cellular and viral proteinases. Virus particles assemble in an LD-associated subregion of the ER and the Golgi apparatus and are released vie the secretory pathway. However, the precise mechanisms involved in the export process are not fully understood yet. HCV virions incorporate not only virus but also host proteins, many of which have been shown to be functionally implicated in the viral life cycle by modulating cellular processes involved in lipid metabolism (Chang *et al.*, 2007) (Huang *et al.*, 2007; Meunier *et al.*, 2008), protein folding (Parent *et al.*, 2009) and others (Benga *et al.*, 2010)

FIG4 is a phosphoinositide (PI) 5'-phosphatase highly specific for Phosphatidylinositol 3,5-bisphosphate ($PI(3,5)P_2$) (Tosch *et al.*, 2006). Mutations in FIG4 lead to neurodegeneration in pale tremor mice and in patients suffering from a specific form of Charcot-Marie-Tooth disease (Chow *et al.*, 2007), familial epilepsia (Baulac *et al.*, 2014) or Yunis-Varón syndrome (Campeau *et al.*, 2013). What is more, altered $PI(3,5)P_2$ synthesis, turnover anddownstream signaling, as well as direct modulation of FIG4, has been shown to have a profound effect on normal endosomal membrane organization and dynamics (Michell *et al.*, 2006). (Ikonomov *et al.*, 2006; Rutherford *et al.*, 2006).

In this study, we identify FIG4 as a novel component of a significant subset of HCV particles and show that it plays an important role in the HCV life cycle by regulating the levels of CE.

## Results & Discussion

### *Identification of FIG4 as an HCV virion-associated protein*

In order to identify host cell factors that associate with circulating HCV virions, we performed a proteomic analysis of HCV particles isolated from the plasma of two viremic patients. Plasma from an aviremic subject served as control After initial pelleting, HCV particles were sedimented on iodixanol gradients via isopycnic centrifugation. Monitoring HCV RNA in the collected fractions identified peaks of viral RNA at 1.04 and 1.17 g/ml of iodixanol. To further decrease the level of non-specific background, we subjected our virus-containing fractions to a second iodixanol gradient-based purification step (Parent *et al.*, 2009). Following HPLC/MS analysis of the virus-containing fractions, we found FIG4 to be significantly enriched in these fractions, but absent from the corresponding aviremic control samples.

In order to confirm the presence of FIG4 on the particles, we immunoprecipitated FIG4 from infected Huh7.5 cells and investigated if we could enrich for HCV RNA. In order to substantiate our results we used a mouse monoclonal and rabbit polyclonal anti-FIG4 antibody obtained from two different suppliers. As expected, our positive control, the human anti-E2 CBH5 monoclonal antibody showed the highest enrichment ratio when compared to an isotype control (Fig.1a). RNA of in vitro produced HCV from either genotype 1 or 2 could be enriched 1.7-fold (Gt2) and about 30-fold (Gt1) (Fig. 1b,c). To confirm these results in a clinical setting, we performed IP-qPCR of using double-fractionated patient plasma. We analysed whole plasma as well as low-density lipoviroparticles (LVP, d<1.05) and the pellet obtained after ultracentrifugation (Fig. 1d). Interestingly, we obtained different enrichment ratios, depending on the fraction analysed and the antibody used for the precipitation. While RNA from high density material only poorly co-precipitated, viral RNA could be enriched from whole plasma using the rabbit polyclonal antibody. Since the rabbitt polyclonal antibody binds the N-terminal domain, while the mouse monoclonal antibody binds the C-terminal domain of FIG4, this suggests that the association of FIG4 with HCV virions is dependent on the overall composition of the viral particles and likely to be lipid sensitive.

To provide further evidence that FIG4 is indeed incorporated into HCV virions, we performed immunogold electron microscopy (IEM) on supernatants of infected Huh7.5 cells. As shown in figure 2 (top row, left image), no virion-like structures were observed in HCV-negative supernatants. The same was true for HCV-positive samples stained with the secondary antibodies only, ruling out non-specific staining (Fig. 2, top row, right image). However, the anti-rabbit secondary antibody produced a weak

background labeling of the grid itself (Fig. 2, medium row, left image). Although labeling was weak, probing HCV-positive supernatants with anti-FIG4 antibodies clearly detected virions 50-70 nm in size, which is characteristic for in vitro-derived viral particles (Catanese *et al.*, 2013) (Fig. 2, middle row, right image; and both images of the bottom row). Not all virions were found to be FIG4-positive. Whether this is linked to an intrinsic heterogeneity of FIG4 expression from one viral particle to another or to the low labeling yield, a common issue of immuno-electron microscopy, is unknown. Of note, ApoE staining in the same context resulted in a similar staining yield as FIG4 (Parent *et al.*, 2009 and data not shown).

Next, we sought to investigate the functional role of virion-associated FIG4. To this end, we pre-incubated cell culture-derived genotype 2 (Gt2 HCVcc) virus particles with anti-FIG4 antibodies and measured changed in infectivity by 50% cell culture infectious dose ($TCID_{50}$) endpoint dilution assay. As expected, the human anti-E2 CBH5 monoclonal antibody drastically reduced HCV infectivity (Suppl. Figure 1a). Preincubation with anti-FIG4 antibodies significantly inhibited HCV infectivity by 40-50% while control antibodies had no effect on the virus (Suppl. Figure 1b). To gain insight into the clinical relevance of our results, we tested virions from an additional genotype 1-infected patient, distinct from the material used for the initial MS analysis. As before, immunogold labeling experiments confirmed the association of FIG4 with the serum-derived HCV particles. Despite the low labeling yield, one to several gold particles were observed per virion when incubated with the anti-FIG4 antibodies (Suppl. Figure 2). Interestingly, the size of FIG4-labeled particles of clinical origin was lower than the one of their in vitro counterparts.

Taken together, we identify and confirm FIG4 as a component of a subset of in vitro- as well as patient derived HCV virions. What is more, FIG4 appears to be exposed on the surface of the virus particle since it is accessible for antibody binding. These results demonstrate that FIG4 associates to HCV virions and may play a moderate role in early interactions of at least a subset of particles with their target cells as found with other virion-bound proteins (Chang *et al.*, 2007) (Parent *et al.*, 2009).

***FIG4 locates in close proximity to the ER and HCV core-positive LDs and modulates viral morphogenesis and infectivity***

To further dissect the role of FIG4 in the viral cycle, we first assessed the effect of reduced FIG4 expression on HCV replication and infectivity. Huh7.5 cells were transfected with two different FIG4-targeting siRNAs and knockdown efficiency tested

by western blot (Suppl. Fig. 3a). SiRNA-mediated cytotoxicity was ruled out after performing Sulforhodamine and Neutral Red assays (Suppl. Fig. 3b and c). As shown in figures 3a and d, FIG4 depletion did not alter intra- and extracellular HCV RNA Gt2 levels. In contrast, intra- and extracellular HCV infectivity was decreased by up to 60 and 75%, respectively (Fig. 3b and e). Similarly, levels of released HCV core levels were also decreased (Fig. 3f). In both cases, siRNA-mediated inhibition could be largely rescued by the addition of exogenous PI3P (Fig. 3c and g).

We used the same approach for a Gt1 virus, except that infectivity assays could not be performed due to the low propagation potential of these strains in vitro. Again, while FIG4 depletion had no impact on intracellular HCV RNA Gt1 levels (Fig. 4a), it did decrease HCV core release in a similar manner as observed for Gt2 (Fig. 4b). Taken together, this data suggests that FIG4 is involved in the viral life cycle downstream of the replication phase.

Next, we investigated the effect of FIG4 overexpression on HCV. To this end we transfected Huh7.5 cells with C-terminal GFP-tagged wild type FIG4 (WT FIG4-GFP) or a phosphatase dead mutant (P.Dead FIG4-GFP) harboring a C488S point mutation in its catalytic domain. GFP-only (Ctrl GFP) served as control plasmid (Suppl. Fig. 4a). As for the siRNA oligos, proper expression and absence of cytotoxic side-effects were verified by western blot and cell viability assays (Suppl. Fig. 4b-d). Three days after plasmid transfection and virus infection, cells were harvested and viral replication and infectivity measured as before. In accordance with our previous data, FIG4 overexpression had no significant effect on overall HCV Gt2 RNA levels (Fig. 5a and c), while a respective 4- and 6-fold increase of intra- and extracellular HCV infectivity was observed when compared to GFP control cells. Expression of phosphatase-dead FIG4-GFP resulted in a weak, yet not statistically significant increase of HCV intracellular infectivity (Fig. 5b) and released HCV core levels (Fig. 5e). As shown in figures 6a and b, similar results were obtained for WT FIG4 and a Gt1 virus. Surprisingly, P.Dead FIG4 increased HCV core releases, although to a lesser extent than the WT construct. Whether this is linked to structural differences in the Gt1 and Gt2 core sequences making the former sensitive to FIG4's backbone for morphogenesis is unknown. Taken together, these results further support the role of FIG4 in the formation of functional HCV particles and suggest that the phosphatase activity of FIG4 is involved in the process.

Virion-bound host proteins often contribute to viral budding, not least due to their specific intracellular location. Using immunofluorescence microscopy we studied the association of FIG4-GFP with a set of organelle- and virus-specific markers. As expected, GFP-only produced a diffuse signal in the cytosol and the nucleus (Suppl. Fig. 5a). In contrast, we observed a distinct punctate staining pattern for FIG4, which did not change, regardless if the cells were infected or not. Indeed, FIG4 appeared to closely associate with the ER marker calnexin (Fig. 7, top row) and oil-red-O stained LDs (Fig. 7, second row). However, we could not confirm the previously published localization of FIG4 to early endosomes labelled with EEA1 (Sbrissa *et al.*, 2007) (Suppl. Fig. 5b). Given that LDs have been shown to be the site of viral morphogenesis and budding, we next looked at the association of FIG4 with HCV core protein and dsRNA in infected cells. HCV core protein associated with LDs can be easily distinguished by virtue of its characteristic doughnut-shaped staining pattern. Interestingly, FIG4 colocalised with LD-associated HCV core (Fig. 7, third row). Likewise, rarer yet visible colocalization was observed between FIG4 and HCV dsRNA complexes (Fig. 7, fourth row). In summary, we show that a substantial fraction of the FIG4 cytosolic pool appears to be located around core-decorated ER/lipid droplet structures which corresponds to HCV assembly sites (Miyanari *et al.*, 2007), arguing for a role of FIG4 in the viral budding processes. SAC1 is an ER-membrane-spanning PI phosphatase, which is involved in the HCV secretion process (Bishe *et al.*, 2012). Interestingly, FIG4 also possesses a catalytic SAC1 domain (Sbrissa *et al.*, 2007). However, despite this similarity, not much is known about the topology. We thus conducted an in silico analysis of FIG4 using the TMHMM Server, Tmpred, SPLIT 4.0 Server, and DAS programs. All four programs identified a potential transmembrane domain ranging from residues 83-105. In addition, FIG4 contains a canonical arginine-based RXRXX motif (namely RNRYL at positions 903-907), a known ER transmembrane retention signal. Overall, this suggests that FIG4 is associated with the ER membrane, which would explain how it is incorportated into the virion during assembly and budding.

Several bacteria and viruses modulate and exploit the host PI metabolism to ensure efficient replication and survival (Delang *et al.*, 2012). Another PI-related enzyme, phosphatidylinositol 4-kinase PI4KIIIα, has also been demonstrated to be crucial for hepatitis C virus replication (Berger *et al.*, 2009; Harak *et al.*, 2014; Trotard *et al.*, 2009). PI4KIIIα appears to be directly recruited and activated by the HCV non-structural protein NS5A protein to the replication complexes (Berger *et al.*, 2009). Other

PI-binding proteins with roles during the HCV life cycle include the oxysterol binding protein (OSBP) which is instrumental for HCV secretion binds PI4P (Amako *et al.*, 2009) and annexin A2, aII of which is required for virus assembly (Backes *et al.*, 2010). HCV morphogenesis/secretion and replication are often differentially regulated. Until recently, only PI4KIIIα products have been implicated in the viral life cycle. Hence, together with a recently published study indicating that PI(4,5)P2 mediates viral genome replication (Cho *et al.*, 2015) our results strengthen the relevance of other, additional species of PIs for HCV propagation.

***FIG4, CE levels and the secretory pathway***

FIG4 is one of the proteins that regulate the concentration of $PI(3,5)P_2$ in eukaryotic cells, a PI involved in the regulation of intracellular organelle trafficking (Dove *et al.*, 2009). Reduction of $PI(3,5)P_2$ in yeast results in the production of enlarged vacuoles due to defects in vacuole fission and retrograde trafficking to the Golgi (Bonangelino *et al.*, 2002), suggesting a potential role of FIG4 in endomembrane trafficking and the secretory pathway. However, nothing is known about its physiological role in hepatocytes. It is noteworthy that none of the pathologic conditions related to FIG4 mutations (Baulac *et al.*, 2014; Chow *et al.*, 2009; Ferguson *et al.*, 2012; Nicholson *et al.*, 2011) are associated with hepatic defects. Nevertheless, to assess if the FIG4-mediated effect on viral infectivity could be due to modulation of the secretory pathway, we first examined the ultrastructure of hepatocytes from FIG4 null mice by TEM. However, no morphological alterations were observed when compared to WT mice (Suppl. Fig. 6). Next, we knocked down FIG4 in Huh7.5 cells and using immunofluorescence, examined various compartments of the secretory pathway, such as the reticular subdomain of the ER (CLIMP63 staining), the intermediate compartment (ERGIC-53 staining) and the Golgi apparatus (GM130 staining). But as shown in supplementary figure 6, no noticeable differences were observed. Next we used a so-called retention using selective hooks (RUSH) assay (Boncompain & Perez, 2013) to test the functionality of the secretory pathway. As before, depletion of FIG4 did not impair the trafficking of secretory cargo between the ER and the Golgi (Suppl. Fig. 7, 8 and 9). Taken together, these results suggest that FIG4 modulatss infectivity through process distinct than secretion.

Given the interplay between PIs and lipids, their previous association with the HCV life cycle, and our observed FIG4-dependent HCV phenotype, we tested if FIG4 could modulate TG and CE levels, two of the main classes of lipids hijacked by HCV for its

own replicative benefit (Alvisi *et al.*, 2011). TG levels and LD volume and numbers remained unaffected by FIG4 knockdown or overexpression (not shown). In contrast, FIG4 depletion reduced cellular CE levels 2 to 3-fold (Fig. 8a), while FIG4 overexpression resulted in a 2 to 3-fold CE increase (Fig. 8b) in naïve as well as infected Huh7.5 cells (Fig. 8c and d, HCV-infected cells). Interestingly, one of the siRNA used (targeting exon 19 at the extreme 3' side of the *Fig4* transcript) did not exert its effect in HCV-infected cells (Fig. 8c), suggesting that an isoform expression switch towards an exon 19 negative FIG4 occurred upon infection. Rescue of infectivity by exogenous PI3P upon RNAi depletion of FIG4 by the both siRNAs strengthens this hypothesis and rules out the likelihood of off-target effects as the source of the phenotype observed. Circulating HCV virus particles resemble very low density lipoprotein-like particles termed lipoviral particles (LVPs), which are enriched for CE (Merz *et al.*, 2011). In addition, HCV infection modulates CE synthesis to facilitate the production of infectious particles. Moreover, inhibition of cholesterol esterification impairs production of infectious virus (Liefhebber *et al.*, 2014; Read *et al.*, 2014). Together, this suggests that FIG4 might affect viral morphogenesis and secretion by modulating levels of CE. However, the FIG4-induced differences in CE levels are independent of its phosphatase activity, suggesting an additional FIG4 mode of action. One cannot rule out the fact that structural features of FIG4 as an enzymatically inert backbone in the case of the phosphatase–dead mutant are sufficient for activation of CE accumulation, while the phosphatase activity is necessary for viral infectivity. Also, isoform switches may occur upon HCV infection (Colman *et al.*, 2013), which could explain the apparent uncoupling of backbone and activity under certain circumstances. As for entry, anti-FIG4 antibodies may either limit access of CE to CE receptors (such as SRB1, LDLR or NPC1) through steric hindrance or may directly impede interactions of FIG4 with putative binding partners. The fact that FIG4 has been shown to colocalize with EEA1 in some instances (Sbrissa *et al.*, 2007) could also mean its involved in post-entry steps at the endosome level.

HCV association with FIG4 clearly provides an advantage for virion production, possibly via FIG4-mediated modulation of CE. As mentioned above, the function of FIG4 in the liver is still unknown. To our knowledge it is also not fully understood how to link PI phosphatases to the cholesterol metabolism. Nevertheless, an increasing number of reports show that PI-mediated signaling events are at least in some cases cholesterol dependent. Interestingly, the PTEN phosphatase influences CE levels through its protein phosphatase activity (Peyrou *et al.*, 2013), and FIG4 may stimulate

CE synthesis possibly by acting also as a protein phosphatase (Duex *et al.*, 2006). Given the importance of CE biology in HCV pathophysiology and VLDL formation (Lambert *et al.*, 2013) (Alvisi *et al.*, 2011), future studies aiming at identifying the molecular bases of this finding are certainly needed.

In summary, this study demonstrates that FIG4/KIAA0274, a recently identified PI phosphatase with a yet unknown function in the liver is an HCV virion component and modulates viral infectivity in a post-replicative fashion, possibly by influencing CE-levels.

## Materials and Methods

### Purification of HCV virions.

Clinical material has been processed under the approval of the french IRB (CPP Sud-Est II, agreement #2010-08-AM2). Infected plasma was obtained from three HCV positive patients and an aviremic control and processed after approval of the french IRB (CPP Sud-Est II, agreement #2010-08-AM2). Plasmas were stabilized with 10mM Hepes (Gibco), antiproteases (Roche), centrifuged at 8,000 *g* for 15 minutes at 4°C, filtered through 0.45 µm membranes, layered onto a 20% sucrose cushion in TNE (10 mM Tris, 150 mM NaCl, 2 mM ethylene diamine tetraacetic acid) and ultracentrifuged at 27,000 rpm for 4 hours at 4°C. Pellets were then resuspended in 1 mL of TNE, layered on top of iodixanol gradients, and submitted to isopycnic ultracentrifugation for 16 hours at 31,200 rpm at 4°C. Fractions were then harvested from the top of the gradient. The amount of HCV RNA in each fraction was determined by real-time polymerase chain reaction (PCR). The fractions with the highest RNA content and the corresponding fractions from the uninfected control were pooled and dialyzed against TNE overnight at 4°C. Fractions were then concentrated 10- to 20-fold in YM-3 concentration devices (Centricon; Millipore, Billerica, MA), submitted to a second ultracentrifugation step and processed for mass spectrometry. Low density material and pelleted material were separated by ultracentrifugation on a 20% sucrose cushion as mentioned above.

### Electron microscopy

Viral suspensions were generated from infected cell supernatants or patient plasma which was clarified and then concentrated on a 20% sucrose cushion as described (Parent *et al.*, 2009). Suspensions were adsorbed on 200 mesh Nickel grids coated with formvar-C for 2 min at room temperature (RT). Immunogold labelling was performed by floating the grids on droplets of reactive media. Grids were blocked in 1% BSA / 1% normal goat serum / 50 mM Tris-HCl, pH 7.4 for 10 min at RT. Incubation with anti-FIG4 primary antibodies (40µg/ml) was carried out in a wet chamber for 2 hours at RT. Following successive washes in 50 mM Tris-HCl, pH 7.4 and pH 8.2 at RT, grids were first incubated in 1% BSA / 50 mM Tris-HCl, pH 8.2 in a wet chamber for 10 min at RT and then labeled with 10nm gold-conjugated IgG (Aurion) diluted 1/80 in 1% BSA / 50 mM Tris-HCl pH 8.2 for 45 min. Grids were then subjected to two washes in 50 mM Tris-HCl pH8.2 and pH 7.4 and finally rinsed in distilled water.

Following a 2 min fixation with 4% glutaraldehyde, grids were stained with 2% phosphotunstic acid for 2 min and then analysed using a transmission electron microscope (Jeol 1400 JEM, Tokyo, Japan) equipped with a Gatan camera (Orius 600) and a Digital Micrograph Software. Mouse work was carried out in agreement with the IRB of the U. of Michigan, using liver pieces derived from other research programs. For standard ultrastructural analysis by EM, cells were treated as described previously (Hourioux *et al.*, 2007).

**Immunofluorescence**

Plasmid or siRNA-transfected Huh7.5 cells were first stained with the primary antibodies (anti-calnexin from Santa Cruz, anti-HCV core C7/50 from Santa Cruz, anti-dsRNA from Scicons and anti-EEA1 (BD Biosciences), all being used at a concentration of 2µg/mL) and then incubated with Alexa-680–conjugated secondary antibodies (4µg/mL). GFP was detected through direct excitation. Lipid droplets were stained using the neutral lipid-specific dye Oil Red O (ORO). Cell nuclei were counterstained with Hoechst 33358 and visualized under a Leica SP5 confocal microscope. Merged images were obtained using the ImageJ software. Bar = 10 µm. White triangles point to regions of interest.

**Cell Culture and HCV Infection.**

The human hepatoma cell line Huh7.5 was cultured in Dulbecco's minimal essential medium (DMEM; Life Technologies) supplemented with 10% fetal bovine serum (FBS; Thermo Scientific) and 1% penicillin-streptomycin (Life Technologies).

Viral stocks were generated via transfection of in vitro transcripts encoding the JFH1 genotype 2a-derived strain (Delgrange *et al.*, 2007). $2x10^4$ cells/$cm^2$ were infected with HCV JFH1 at an MOI of 0.1. HCV genotype 1 RNA derived from H77 and N strains was electroporated as described in (Blight *et al.*, 2002).

**Immunoprecipitation and Neutralization Assays**

Supernatants from infected cells were harvested 4 days post infection, cleared by centrifugation and then supplemented with 10mM HEPES and protease-inhibitors. Immunoprecipitation of secreted virions with antibodies coupled to protein G magnetic beads (2µg/IP) was carried out as described previously (Jammart *et al.*, 2013). Material was then subjected to RNA extraction (Qiagen) and RT-qPCR. For neutralization assays, supernatants from infected cells were harvested 4 days post infection and then

incubated overnight with anti-FIG4 sc-98633 (Santa Cruz Biotechnology), anti-FIG4 N202/7 (Neuromab), anti-HCV E2 clone CBH5 (obtained from S. Foung), an isotype-matched anti-R04 control antibody, or rabbit and mouse Igs (Sigma) at a final concentration of 0.4 or 2 or 10 µg/mL (except for anti-HCV E2 antibody that was used at a final concentration of 0.02; 0.1 and 0.5 µg/mL). Infection of naïve Huh7.5 cells seeded the day before at a density of twenty thousand cells per square centimeter was performed for three days. An HCV infectivity assay is then performed.

**HCV infectivity Assay**

Cells were seeded in 96-well plates (6,400/well) the day before infection. Cells were then inoculated with 10-fold serial dilutions of the supernatants of interest. 96 hours post infection, cells were washed with PBS, fixed for 10 minutes in methanol/acetone and blocked for 30 minutes in 1X PBS / 5% BSA. Cells were then probed with in-house HCV antiserum (1/500) in 1X PBS / 3% BSA for 1 hour at RT. After three washes in 1X PBS / 3% BSA, bound primary antibodies were probed with 1 µg/mL goat anti-human Alexa Fluor 488 secondary antibodies (Life Technologies) for 1 hour at room temperature and visualized by epifluorescence (Nikon TE2000E). Viral titers were determined using the adapted Reed and Münch method (Lindenbach, 2009).

**Cloning of FIG4 constructs**

The full-length FIG4 ORF (GenBank acc.# NM_014845.5) was inserted into the pcDNA3 backbone in frame with a C-terminal GFP tag using a restriction-ligation reaction of *SacII* and *AgeI* sites. The same strategy was used for the phosphatase dead mutant bearing the C486S mutation (a gift from M. Meisler, U. of Michigan). Final plasmids were verified by sequencing.

**FIG4 overexpression and siRNA-mediated knockdown**

Subconfluent Huh7.5 cells were transferred to an electroporation cuvette (BioRad GenePulser Xcell Electroporation Systems) and then mixed with either 10µg of plasmid DNA or 8 nM of siRNA (NT siRNA, siRNA Fig4 #5 [Hs_KIAA0274_5 from QIAGEN], siRNA FIG4 #6 [Hs_KIAA0274_6 from QIAGEN]. Cells were then electroporated with one pulse at 140 V, 125Ω, and 2300 µF. After electroporation, cells were allowed to recover at RT for 5 min and then resuspended in complete DMEM and plated in 6-well plates. For the siRNA rescue experiment, 5µM PI3P (Sigma) was added to the cells.

**HCV core protein quantification**

HCV core concentration in the supernatant of infected cells was quantified using the QuickTiter™ HCV Core Antigen ELISA Kit (CELL BIOLABS).

**Neutral Red assay**

The NR stock solution (40mg NR dye in 10 mL PBS) was diluted in culture medium to a final concentration of 4 mg/ml and then centrifuged at 600g for 10 min to remove any precipitated dye crystals. Cells were then incubated with 100 µL of NR medium for 1 h. NR medium was removed and the cells washed with PBS. Plates were incubated for 10 min under shaking with 150 µL/well of NR destain solution (50% ethanol 96%, 49% deionized water, 1% glacial acetic acid). OD was measured at 540 nm in a microplate spectrophotometer.

**Sulforhodamine assay**

Cells were incubated with 100 µL of 0.057% Sulforhodamine (SRB) at RT for 30 min and then rinsed four times with 1% acetic acid, followed by four washes with distilled water Plates were left to dry at RT and then incubated in 200 µL 10 mM Tris pH 10.5. Plates were placed on an orbital shaker for 5 min and OD measured at 510 nm in a microplate reader.

**Quantitative RT–PCR**

Total RNA was extracted using trizol (Invitrogen). 1 µg of RNA was DNAse I-digested (Promega) and then reverse transcribed using MMLV reverse transcriptase (Invitrogen) according to the manufacturer's instructions. Quantitative real-time PCR was performed on a LightCycler 480 device (Roche) using the iQ™ SYBR®Green Supermix (BIO-RAD). PCR primer sequences and qPCR conditions are reported in Supplementary Table 1.

**CE quantitation**

Cells were harvested 3 days after transfection and CE amounts were analyzed using the CE Quantitation Kit (Calbiochem Cat. No 428901).

**Acknowledgments**

FIG4 constructs were a gift from M. Meisler (U. of Michigan). We thank T. Wakita (U. of Tokyo, Japan) and C. Wychowski for the gift of the JFH1 adapted strain, as well as C.M. Rice and S. Lemon for the gift of H77 and N strains. We also thank E. Piver, JC. Meunier and P. Roingeard (U. of Tours, France) as well as E. Errazuriz-Cerda, A. Bouchardon (Ciqle, Université Lyon 1) and S. Conzelmann for excellent technical assistance with confocal / electron microscopy and CE samples. We are indebted to J. Trouilleux, I. Delfour and M. Conti for their help with patient samples as well as to CA. Eberle for discussion. This work has been funded by the EU Marie Curie International Reintegration Program (Grant #248364 to RP) the Lyric consortium (FZ, RP) and the ANRS (Grant #2011-031) to RP. JC is a recipient of an ANRS post-doctoral fellowship.

## References


**Aizaki, H., Lee, K. J., Sung, V. M., Ishiko, H. & Lai, M. M. (2004).** Characterization of the hepatitis C virus RNA replication complex associated with lipid rafts. *Virology* **324**, 450-461.

**Alvisi, G., Madan, V. & Bartenschlager, R. (2011).** Hepatitis C virus and host cell lipids: an intimate connection. *RNA biology* **8**, 258-269.

**Amako, Y., Sarkeshik, A., Hotta, H., Yates, J., 3rd & Siddiqui, A. (2009).** Role of oxysterol binding protein in hepatitis C virus infection. *J Virol* **83**, 9237-9246.

**Backes, P., Quinkert, D., Reiss, S., Binder, M., Zayas, M., Rescher, U., Gerke, V., Bartenschlager, R. & Lohmann, V. (2010).** Role of annexin A2 in the production of infectious hepatitis C virus particles. *Journal of virology* **84**, 5775-5789.

**Bartenschlager, R., Penin, F., Lohmann, V. & Andre, P. (2011).** Assembly of infectious hepatitis C virus particles. *Trends Microbiol* **19**, 95-103.

**Baulac, S., Lenk, G. M., Dufresnois, B., Ouled Amar Bencheikh, B., Couarch, P., Renard, J., Larson, P. A., Ferguson, C. J., Noe, E., Poirier, K., Hubans, C., Ferreira, S., Guerrini, R., Ouazzani, R., El Hachimi, K. H., Meisler, M. H. & Leguern, E. (2014).** Role of the phosphoinositide phosphatase FIG4 gene in familial epilepsy with polymicrogyria. *Neurology* **82**, 1068-1075.

**Benga, W. J., Krieger, S. E., Dimitrova, M., Zeisel, M. B., Parnot, M., Lupberger, J., Hildt, E., Luo, G., McLauchlan, J., Baumert, T. F. & Schuster, C. (2010).** Apolipoprotein E interacts with hepatitis C virus nonstructural protein 5A and determines assembly of infectious particles. *Hepatology* **51**, 43-53.

**Berger, K. L., Cooper, J. D., Heaton, N. S., Yoon, R., Oakland, T. E., Jordan, T. X., Mateu, G., Grakoui, A. & Randall, G. (2009).** Roles for endocytic trafficking and phosphatidylinositol 4-kinase III alpha in hepatitis C virus replication. *Proceedings of the National Academy of Sciences of the United States of America* **106**, 7577-7582.

**Bishe, B., Syed, G. H., Field, S. J. & Siddiqui, A. (2012).** Role of phosphatidylinositol 4-phosphate (PI4P) and its binding protein GOLPH3 in hepatitis C virus secretion. *J Biol Chem* **287**, 27637-27647.

**Blight, K. J., McKeating, J. A. & Rice, C. M. (2002).** Highly permissive cell lines for subgenomic and genomic hepatitis C virus RNA replication. *Journal of virology* **76**, 13001-13014.

**Bonangelino, C. J., Nau, J. J., Duex, J. E., Brinkman, M., Wurmser, A. E., Gary, J. D., Emr, S. D. & Weisman, L. S. (2002).** Osmotic stress-induced increase of phosphatidylinositol 3,5-bisphosphate requires Vac14p, an activator of the lipid kinase Fab1p. *J Cell Biol* **156**, 1015-1028.

**Boncompain, G. & Perez, F. (2013).** Fluorescence-based analysis of trafficking in mammalian cells. *Methods in cell biology* **118**, 179-194.

**Campeau, P. M., Lenk, G. M., Lu, J. T., Bae, Y., Burrage, L., Turnpenny, P., Roman Corona-Rivera, J., Morandi, L., Mora, M., Reutter, H., Vulto-van Silfhout, A. T., Faivre, L., Haan, E., Gibbs, R. A., Meisler, M. H. & Lee, B. H. (2013).** Yunis-Varon syndrome is caused by mutations in FIG4, encoding a phosphoinositide phosphatase. *American journal of human genetics* **92**, 781-791.

**Catanese, M. T., Uryu, K., Kopp, M., Edwards, T. J., Andrus, L., Rice, W. J., Silvestry, M., Kuhn, R. J. & Rice, C. M. (2013).** Ultrastructural analysis of hepatitis C virus particles. *Proceedings of the National Academy of Sciences of the United States of America* **110**, 9505-9510.

**Chang, K. S., Jiang, J., Cai, Z. & Luo, G. (2007).** Human apolipoprotein e is required for infectivity and production of hepatitis C virus in cell culture. *Journal of virology* **81**, 13783-13793.

**Cho, N. J., Lee, C., Pang, P. S., Pham, E. A., Fram, B., Nguyen, K., Xiong, A., Sklan, E. H., Elazar, M., Koytak, E. S., Kersten, C., Kanazawa, K. K., Frank, C. W. & Glenn, J. S. (2015).** Phosphatidylinositol 4,5-Bisphosphate Is an HCV NS5A Ligand and Mediates Replication of the Viral Genome. *Gastroenterology* **148**, 616-625.

**Chow, C. Y., Landers, J. E., Bergren, S. K., Sapp, P. C., Grant, A. E., Jones, J. M., Everett, L., Lenk, G. M., McKenna-Yasek, D. M., Weisman, L. S., Figlewicz, D., Brown, R. H. & Meisler, M. H. (2009).** Deleterious variants of FIG4, a phosphoinositide phosphatase, in patients with ALS. *American journal of human genetics* **84**, 85-88.

**Chow, C. Y., Zhang, Y., Dowling, J. J., Jin, N., Adamska, M., Shiga, K., Szigeti, K., Shy, M. E., Li, J., Zhang, X., Lupski, J. R., Weisman, L. S. & Meisler, M. H. (2007).** Mutation of FIG4

causes neurodegeneration in the pale tremor mouse and patients with CMT4J. *Nature* **448**, 68-72.

**Colman, H., Le Berre-Scoul, C., Hernandez, C., Pierredon, S., Bihouee, A., Houlgatte, R., Vagner, S., Rosenberg, A. R. & Feray, C. (2013).** Genome-wide analysis of host mRNA translation during hepatitis C virus infection. *Journal of virology* **87**, 6668-6677.

**Delang, L., Paeshuyse, J. & Neyts, J. (2012).** The role of phosphatidylinositol 4-kinases and phosphatidylinositol 4-phosphate during viral replication. *Biochem Pharmacol* **84**, 1400-1408.

**Delgrange, D., Pillez, A., Castelain, S., Cocquerel, L., Rouille, Y., Dubuisson, J., Wakita, T., Duverlie, G. & Wychowski, C. (2007).** Robust production of infectious viral particles in Huh-7 cells by introducing mutations in hepatitis C virus structural proteins. *J Gen Virol* **88**, 2495-2503.

**Dove, S. K., Dong, K., Kobayashi, T., Williams, F. K. & Michell, R. H. (2009).** Phosphatidylinositol 3,5-bisphosphate and Fab1p/PIKfyve underPPIn endo-lysosome function. *Biochem J* **419**, 1-13.

**Duex, J. E., Nau, J. J., Kauffman, E. J. & Weisman, L. S. (2006).** Phosphoinositide 5-phosphatase Fig 4p is required for both acute rise and subsequent fall in stress-induced phosphatidylinositol 3,5-bisphosphate levels. *Eukaryotic cell* **5**, 723-731.

**Egger, D., Wolk, B., Gosert, R., Bianchi, L., Blum, H. E., Moradpour, D. & Bienz, K. (2002).** Expression of hepatitis C virus proteins induces distinct membrane alterations including a candidate viral replication complex. *Journal of virology* **76**, 5974-5984.

**El-Serag, H. B. (2012).** Epidemiology of viral hepatitis and hepatocellular carcinoma. *Gastroenterology* **142**, 1264-1273 e1261.

**Ferguson, C. J., Lenk, G. M., Jones, J. M., Grant, A. E., Winters, J. J., Dowling, J. J., Giger, R. J. & Meisler, M. H. (2012).** Neuronal expression of Fig4 is both necessary and sufficient to prevent spongiform neurodegeneration. *Hum Mol Genet* **21**, 3525-3534.

**Harak, C., Radujkovic, D., Taveneau, C., Reiss, S., Klein, R., Bressanelli, S. & Lohmann, V. (2014).** Mapping of functional domains of the lipid kinase phosphatidylinositol 4-kinase type III alpha involved in enzymatic activity and hepatitis C virus replication. *J Virol* **88**, 9909-9926.

**Hourioux, C., Patient, R., Morin, A., Blanchard, E., Moreau, A., Trassard, S., Giraudeau, B. & Roingeard, P. (2007).** The genotype 3-specific hepatitis C virus core protein residue phenylalanine 164 increases steatosis in an in vitro cellular model. *Gut* **56**, 1302-1308.

**Huang, H., Sun, F., Owen, D. M., Li, W., Chen, Y., Gale, M., Jr. & Ye, J. (2007).** Hepatitis C virus production by human hepatocytes dependent on assembly and secretion of very low-density lipoproteins. *Proceedings of the National Academy of Sciences of the United States of America* **104**, 5848-5853.

**Ikonomov, O. C., Sbrissa, D. & Shisheva, A. (2006).** Localized PtdIns 3,5-P2 synthesis to regulate early endosome dynamics and fusion. *Am J Physiol Cell Physiol* **291**, C393-404.

**Jammart, B., Michelet, M., Pecheur, E. I., Parent, R., Bartosch, B., Zoulim, F. & Durantel, D. (2013).** VLDL-producing and HCV-replicating HepG2 cells secrete no more LVP than VLDL-deficient Huh7.5 cells. *Journal of virology*.

**Lambert, J. E., Bain, V. G., Ryan, E. A., Thomson, A. B. & Clandinin, M. T. (2013).** Elevated lipogenesis and diminished cholesterol synthesis in patients with hepatitis C viral infection compared to healthy humans. *Hepatology* **57**, 1697-1704.

**Liefhebber, J. M., Hague, C. V., Zhang, Q., Wakelam, M. J. & McLauchlan, J. (2014).** Modulation of triglyceride and cholesterol ester synthesis impairs assembly of infectious hepatitis C virus. *J Biol Chem* **289**, 21276-21288.

**Lindenbach, B. D. (2009).** Measuring HCV infectivity produced in cell culture and in vivo. *Methods in molecular biology* **510**, 329-336.

**Merz, A., Long, G., Hiet, M. S., Brugger, B., Chlanda, P., Andre, P., Wieland, F., Krijnse-Locker, J. & Bartenschlager, R. (2011).** Biochemical and morphological properties of hepatitis C virus particles and determination of their lipidome. *The Journal of biological chemistry* **286**, 3018-3032.

**Meunier, J. C., Russell, R. S., Engle, R. E., Faulk, K. N., Purcell, R. H. & Emerson, S. U. (2008).** Apolipoprotein c1 association with hepatitis C virus. *J Virol* **82**, 9647-9656.

**Michell, R. H., Heath, V. L., Lemmon, M. A. & Dove, S. K. (2006).** Phosphatidylinositol 3,5-bisphosphate: metabolism and cellular functions. *Trends in biochemical sciences* **31**, 52-63.

**Miyanari, Y., Atsuzawa, K., Usuda, N., Watashi, K., Hishiki, T., Zayas, M., Bartenschlager, R., Wakita, T., Hijikata, M. & Shimotohno, K. (2007).** The lipid droplet is an important organelle for hepatitis C virus production. *Nature cell biology* **9**, 1089-1097.

**Nicholson, G., Lenk, G. M., Reddel, S. W., Grant, A. E., Towne, C. F., Ferguson, C. J., Simpson, E., Scheuerle, A., Yasick, M., Hoffman, S., Blouin, R., Brandt, C., Coppola, G., Biesecker, L. G., Batish, S. D. & Meisler, M. H. (2011).** Distinctive genetic and clinical features of CMT4J: a severe neuropathy caused by mutations in the PI(3,5)P(2) phosphatase FIG4. *Brain* **134**, 1959-1971.

**Parent, R., Qu, X., Petit, M. A. & Beretta, L. (2009).** The heat shock cognate protein 70 is associated with hepatitis C virus particles and modulates virus infectivity. *Hepatology* **49**, 1798-1809.

**Paul, D., Hoppe, S., Saher, G., Krijnse-Locker, J. & Bartenschlager, R. (2013).** Morphological and biochemical characterization of the membranous hepatitis C virus replication compartment. *J Virol* **87**, 10612-10627.

**Peyrou, M., Clement, S., Maier, C., Bourgoin, L., Branche, E., Conzelmann, S., Kaddai, V., Foti, M. & Negro, F. (2013).** PTEN protein phosphatase activity regulates hepatitis C virus secretion through modulation of cholesterol metabolism. *J Hepatol* **59**, 420-426.

**Read, S. A., Tay, E., Shahidi, M., George, J. & Douglas, M. W. (2014).** Hepatitis C virus infection mediates cholesteryl ester synthesis to facilitate infectious particle production. *J Gen Virol* **95**, 1900-1910.

**Rutherford, A. C., Traer, C., Wassmer, T., Pattni, K., Bujny, M. V., Carlton, J. G., Stenmark, H. & Cullen, P. J. (2006).** The mammalian phosphatidylinositol 3-phosphate 5-kinase (PIKfyve) regulates endosome-to-TGN retrograde transport. *J Cell Sci* **119**, 3944-3957.

**Sbrissa, D., Ikonomov, O. C., Fu, Z., Ijuin, T., Gruenberg, J., Takenawa, T. & Shisheva, A. (2007).** Core protein machinery for mammalian phosphatidylinositol 3,5-bisphosphate synthesis and turnover that regulates the progression of endosomal transport. Novel Sac phosphatase joins the ArPIKfyve-PIKfyve complex. *The Journal of biological chemistry* **282**, 23878-23891.

**Tosch, V., Rohde, H. M., Tronchere, H., Zanoteli, E., Monroy, N., Kretz, C., Dondaine, N., Payrastre, B., Mandel, J. L. & Laporte, J. (2006).** A novel PtdIns3P and PtdIns(3,5)P2 phosphatase with an inactivating variant in centronuclear myopathy. *Hum Mol Genet* **15**, 3098-3106.

**Trotard, M., Lepere-Douard, C., Regeard, M., Piquet-Pellorce, C., Lavillette, D., Cosset, F. L., Gripon, P. & Le Seyec, J. (2009).** Kinases required in hepatitis C virus entry and replication highlighted by small interference RNA screening. *FASEB J* **23**, 3780-3789.

## Figure legends

### Figure 1

**Immunoprecipitation of HCV virion-associated FIG4.**

HCV-positive cell supernatants or human plasma were subjected to immunoprecipitation using the indicated antibodies. RNA was extracted and analysed by RT-qPCR. (a,b) Huh7.5 cells infected with Gt2 HCVcc . (c) Huh7.5 cells electroporated with HCV Gt1 RNA derived from H77 or N strains (d) HCV positive patient plasma. Whole plasma, low density fractions and pellet were used for the immunoprecipitation with FIG4 antibodies. Mann-Whitney, $P<0.05$(*).

### Figure 2

**Association of FIG4 with cell culture-derived HCV particles.** Concentrated supernatants of infected Huh7.5 cells were deposited onto grids and processed for immunogold labeling using the indicated primary antibodies. Bound antibodies were detected using secondary antibodies conjugated to 10-nm gold particles. White arrows depict bound gold particles in lower magnification images. Gold particles located ≤ 40nm (corresponding to a single immunoglobulin length) away from the virion were considered specifically bound. Pictures are representative of two labeling procedures.

### Figure 3

**FIG4 depletion decreases HCV Gt2 infectivity.**

Naïve Huh7.5 cells were transfected with two different siRNAs directed against FIG4 and then infected with Gt2 HCVcc. Supernatants and cells were harvested 72hrs post-electroporation and viral RNA quantified by RT–qPCR (a and d). Intracellular and extracellular HCV infectivity was determined by $TCID_{50}$ (b and e). Decreased infectivity due to FIG4 knockdown can be rescued by supplementing PI3P, the product of FIG4. Cells are treated with 5µM of PI3P immediately after transfection. Infectivity was determined by $TCID_{50}$ 72h post electroporation (c and g). (f) HCV core protein levels 3 days post transfection quantified by ELISA (n=3 +/-sd). Mann-Whitney, $P<0.05$(*), $<0.01$(**), $<0.001$(***).

### Figure 4

**FIG4 depletion decreases HCV Gt1 secretion.**

Naïve Huh7.5 cells were transfected with two different siRNAs directed against FIG4 and then electroporated with in vitro transcribed HCV Gt1 RNA. (a) Intracellular HCV RNA levels were measured by RT–qPCR. (b) HCV core protein levels 3 days post transfection quantified by ELISA (n=3 replicates +/-sd). Mann-Whitney, P<0.05(*).

**Figure 5**

**FIG4 overexpression increases Gt2 HCVcc infectivity in a PtdIn(3,5)$P_2$ phosphatase-dependent manner.**

Naïve Huh7.5 cells were transfected with plasmids expressing the GFP tag (Ctrl GFP), wild type FIG4 (WT Fig4-GFP), or phosphatase dead FIG4 (P.Dead FIG4-GFP) and infected with HCVcc Gt2 the same day. Supernatants and cells were harvested 3 days post infection and RNA levels and viral titers determined by RT-qPCR and $TCID_{50}$, respectively. (a and b) Intracellular and extracellular HCV RNA levels. (b and d) Intracellular and extracellular HCV infectivity (e) HCV core protein levels 3 days post transfection quantified by ELISA (n=3 +/-sd). Mann-Whitney, P<0.05(*), <0.01(**).

**Figure 6**

**FIG4 overexpression increases HCV Gt1 infectivity.**

Naïve Huh7.5 cells were electroporated with plasmids expressing the GFP tag (Ctrl GFP), wild type FIG4 (WT Fig4-GFP), or phosphatase dead FIG4 (P.Dead FIG4-GFP) and with HCV Gt1. Cells and supernatants were harvested 3 days post infection (a) intracellular RNA as determined by RT-qPCR (b) Secreted HCV core protein levels quantified by ELISA (n=3 replicates +/-sd). Mann-Whitney, P<0.05(*), <0.01(**), <0.001(***).

**Figure 7**

**FIG4 is located in the immediate vicinity of HCV core-coated lipid droplets.**

FIG4-GFP-expressing Huh7.5 cells were stained with the indicated antibodies. LDs were visualized using the neutral lipid-specific dye ORO. Cells were counterstained with Hoechst 33358. Merged images were obtained using the ImageJ software. White triangles point to regions of interest. Images are representative for two to three independent experiments.

**Figure 8**

**FIG4 affects cholesteryl esters levels.**

Huh7.5 cells were transfected with the indicated plasmids or siRNA oligos and then infected with Gt2 HCVcc or left uninfected. Cells were harvested 3 days later and CE levels analyzed using the CE Quantitation Kit. (a and c) RNAi-mediated FIG4 knockdown (b and d) FIG4 overexpression (b and d) (n=2 +/-sd). Panels a and b correspond to non-infected cells. Panels c and d correspond to HCV-positive cells. Mann-Whitney, P<0.05(*).

**Supplementary Figure 1**

**HCV neutralization by anti-FIG4 antibodies.**

Gt2 HCVcc virions were incubated with increasing concentrations of antibody and then used to infect naïve Huh7.5 cells. 3 days post infection Infectivity was determined by $TCID_{50}$ and percent relative to the isotype control calculated. (a) Anti-E2 CBH5. Black 0.02µg/mL; grey 0.1µg/mL; light grey 0.5µg/mL (b) two different FIG4 antibodies (FIG4 sc-98633 or FIG4 N202/7), R04 isotype control, rabbit or mouse control Igs. Black 0.4µg/mL; grey 2µg/mL; light grey 10µg/mL. (n=3 +/-sd). Mann-Whitney, P<0.05(*), <0.01(**), <0.001(***).

**Supplementary Figure 2**

**Association of FIG4 with HCV particles concentrated from patient plasma.** Immunogold electron microscopy of concentrated HCV Gt1-positive patient plasma. Bottom panel: Silver amplification was used to achieve a higher labeling rate. Gold particles located ≤40nm (corresponding to a single Ig length) from the virion were considered specific. Pictures are representative of two labeling procedures.

**Supplementary Figure 3**

**FIG4 depletion does not alter cell viability.**

Naïve Huh7.5 cells were transfected with the indicated siRNA oligos and subsequently infected. Knockdown efficiency was determined by Western blot 72 h post transfection. Cell viability 24, 48 and 72 h post transfection as determined by sulforhodamine (b) and Neutral Red assay (c). Doxo, doxorubicin (1µg/ml) was used as a death-inducing control (n=3 +/-sd).

**Supplementary Figure 4**

**FIG4 overexpression does not alter cell viability.**

(a) Physical maps of the ORFs used in the study. (b) FIG4 expression levels 3 days post transfection with the indicated plasmids (c and d) Cell viability of transfected cells as determined by Sulforhodamine (c) and Neutral Red assays (d) (n=3 +/-sd).

**Supplementary Figure 5**

**FIG4 does not colocalize with the early endosome labelled by EEA1**.

Immunofluorescence microscopy of FIG4-GFP-expressing Huh7.5 cells stained with an anti-EEA1 antibody. Cells were counterstained with Hoechst 33358. Merged images were obtained using the ImageJ software. Bar = 10 µm. Images are representative for two to three independent experiments.

**Supplementary Figure 6**

**FIG4 knock-out mice exhibit normal hepatocyte and ER ultrastructure.**

WT and FIG4 null mice livers were submitted to fixation in glutaraldehyde and processed for TEM prior to contrasting with uranyl acetate. Magnification: 10k.

**Supplementary Figure 7**

**FIG4 knockdown does not alter integrity of the secretory pathway.**

Huh7.5 cells were transfected with the indicated siRNAs. Structural and functional integrity of the secretory pathway was analysed using the indicated stains or the RUSH assay. (a) GM130/MannII-GFP; (b) ERGIC53 and (c) CLIMP63; (d) RUSH assay (n=2 +/-sd).

**Supplementary Figure 8**

**Functionality of the secretory pathway is unaltered by FIG4 depletion.**

Huh7.5 cells were transfected with the indicated siRNAs. Colocalization GM130 and MannII-GFP is shown for each condition at baseline and 18 min post displacement (n=2).

**Supplementary Figure 9**

**Functionality of the secretory pathway is unaltered by FIG4 depletion.**

Quantification of optical data obtained in suppl. figure 3 (n=2 +/-sd).

**Supplementary Table 1.**

Primer sequences.

742

figure

Fig. 1

Click here to download Figure: Figure 1 Cottarel et al..pdf

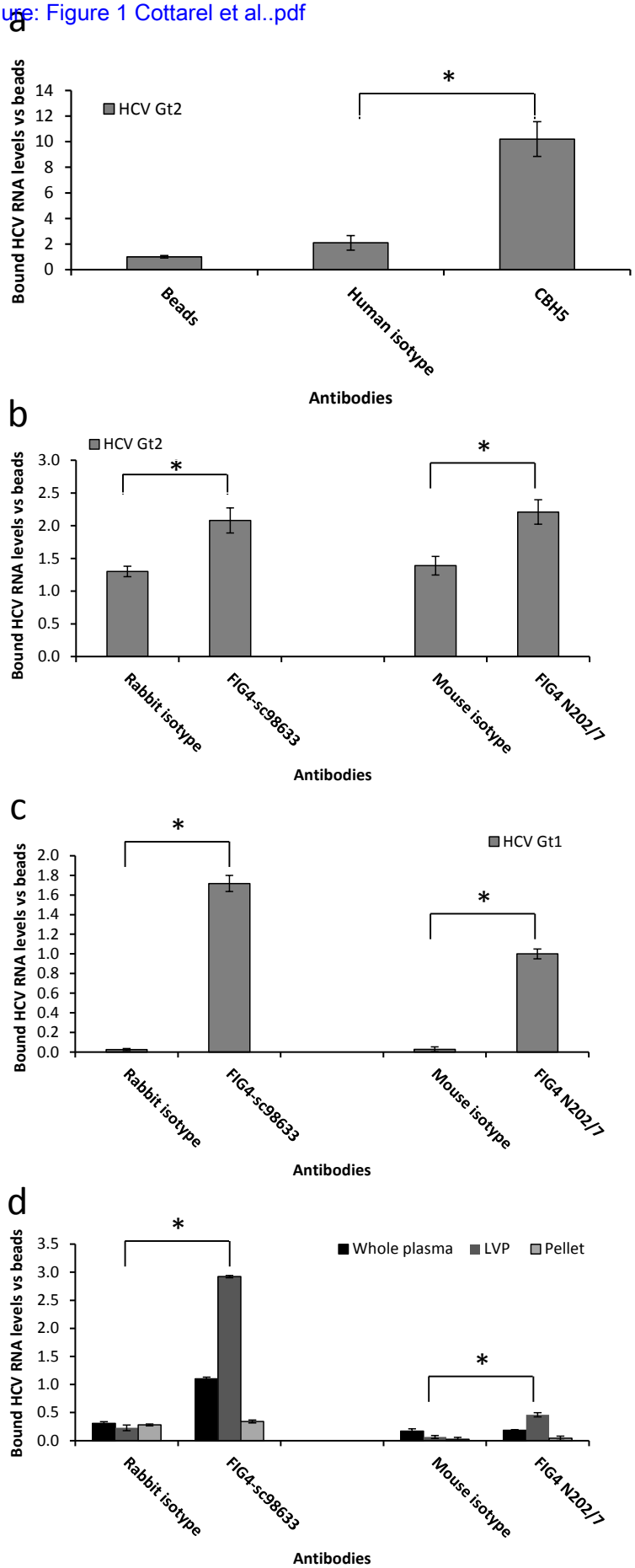

figure

Fig. 2

Click here to download Figure: Figure 2 Cottarel et al..pdf

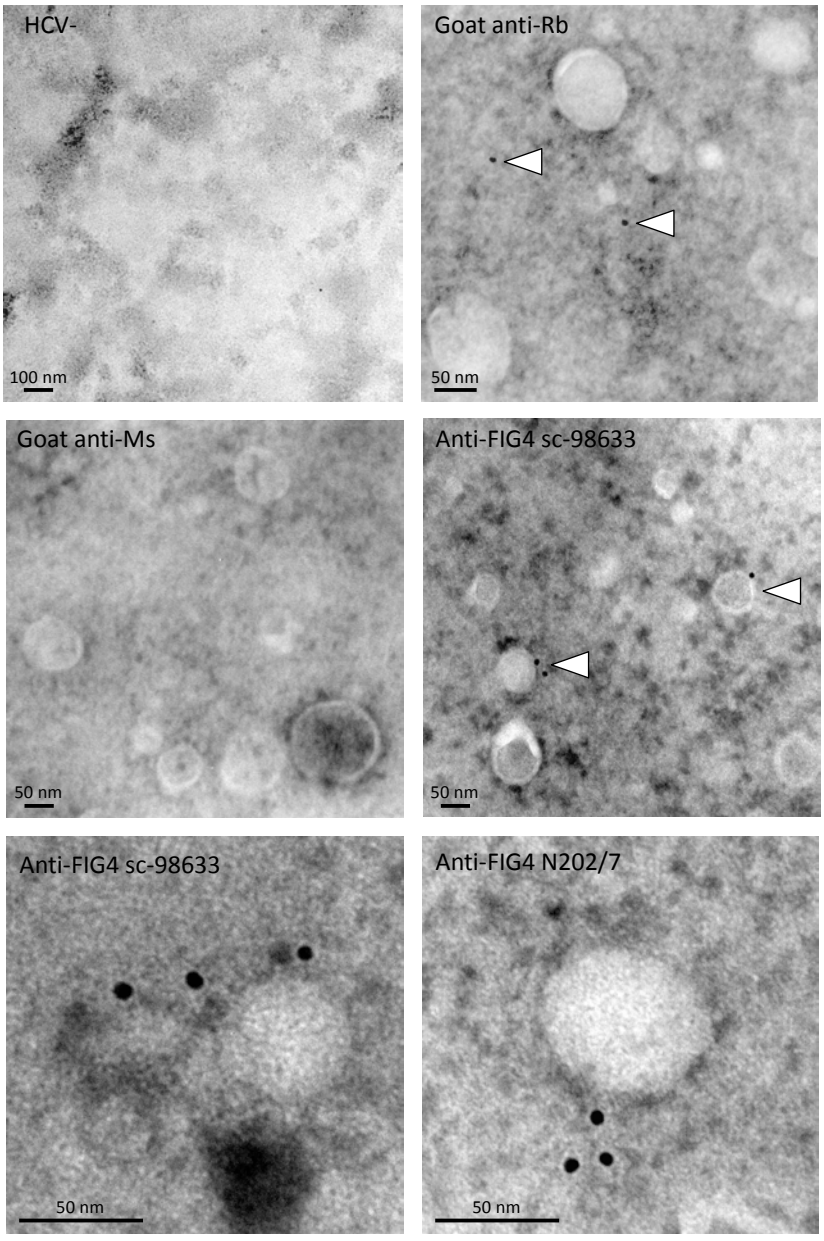

figure
Fig. 3
Click here to download Figure: Figure 3 Cottarel et al..pdf

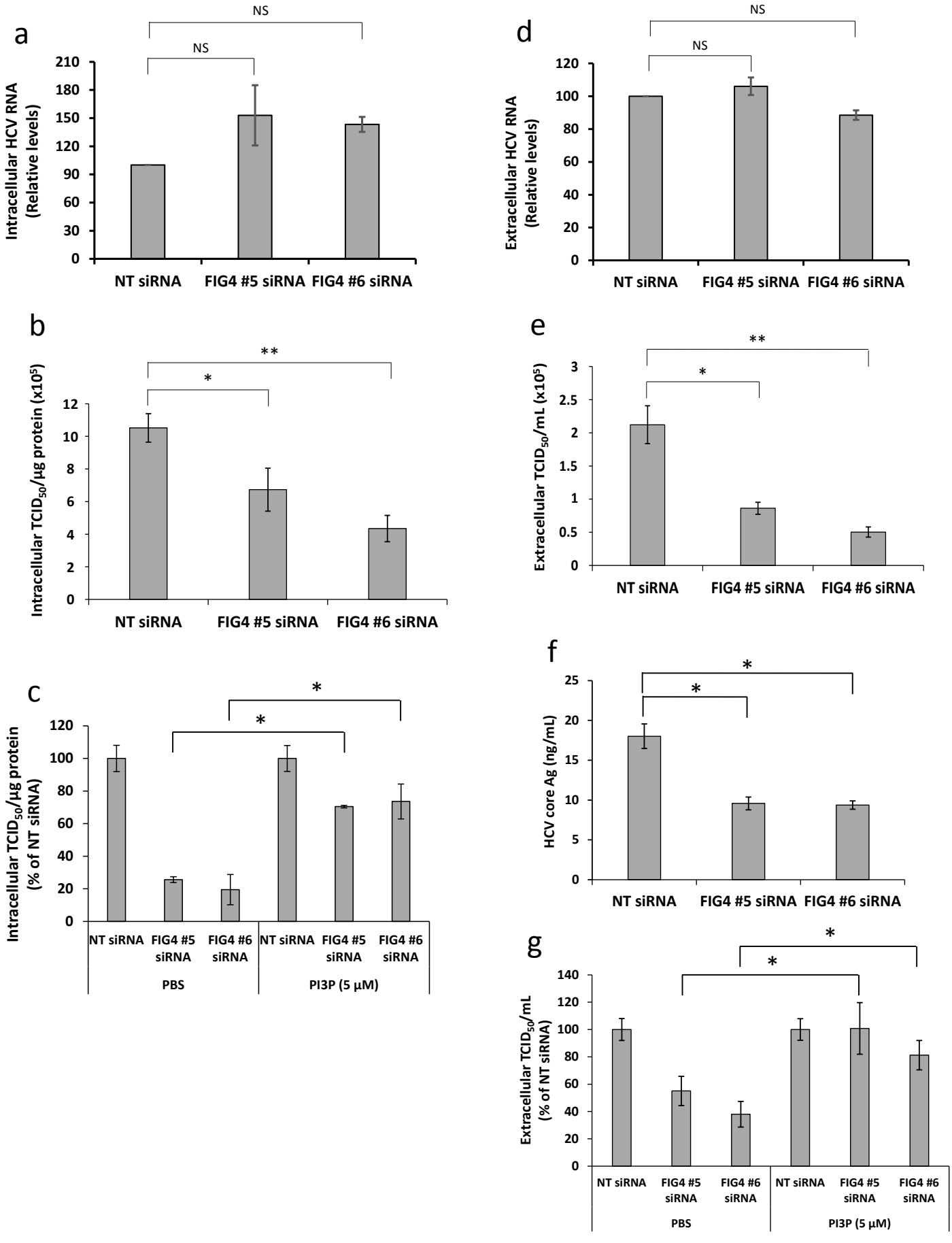

figure
Fig. 4
Click here to download Figure: Figure 4 Cottarel et al..pdf

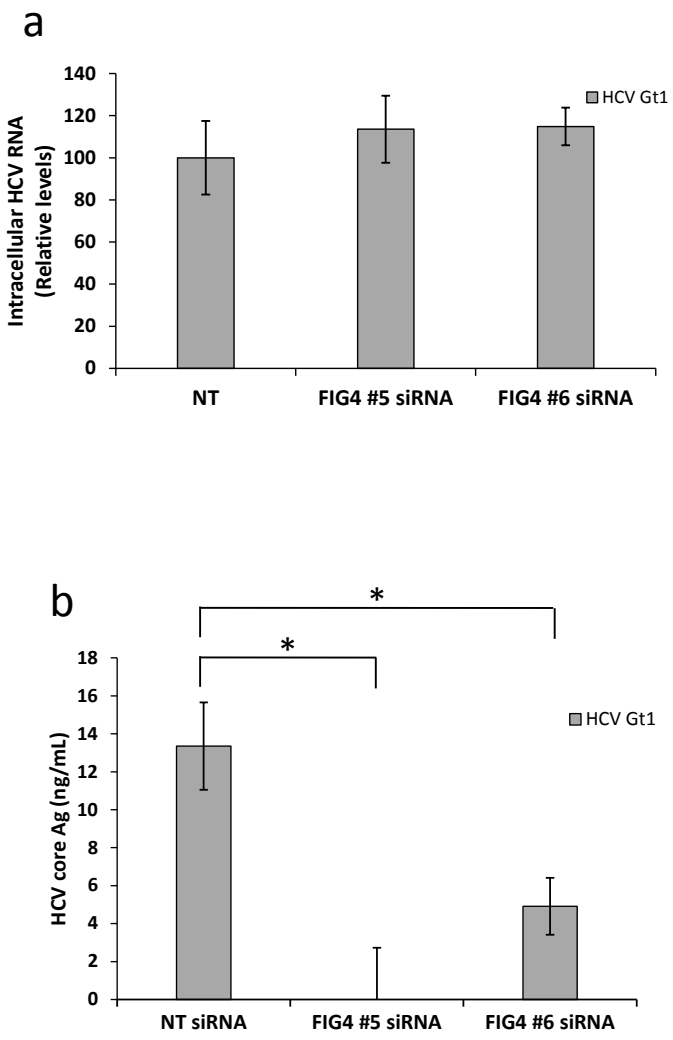

figure
Fig. 5
Click here to download Figure: Figure 5 Cottarel et al..pdf

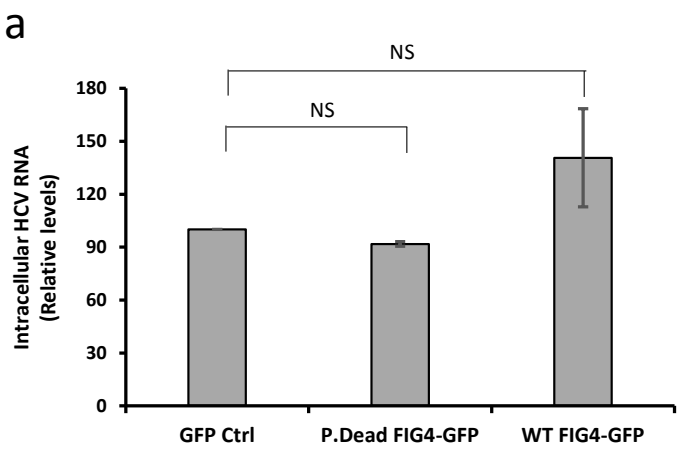


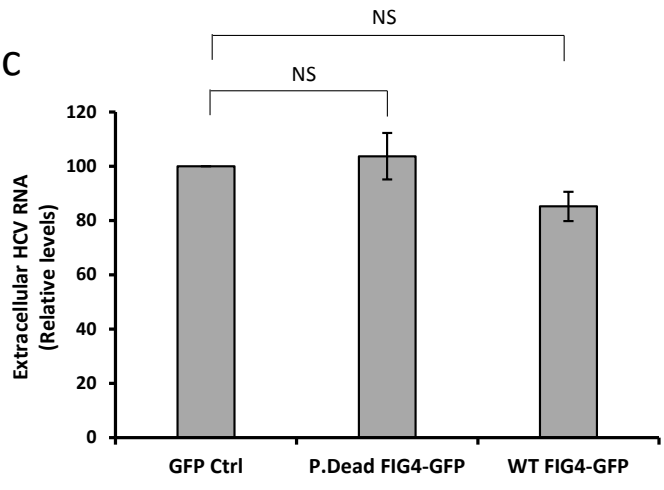


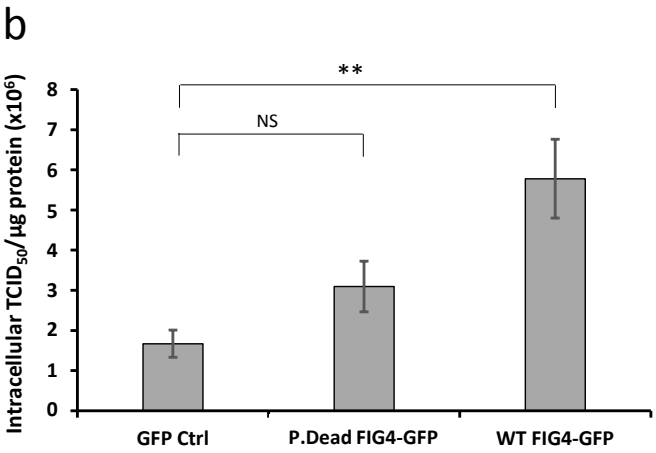


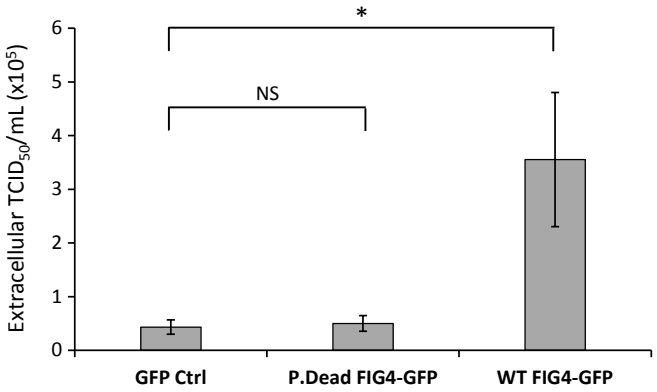


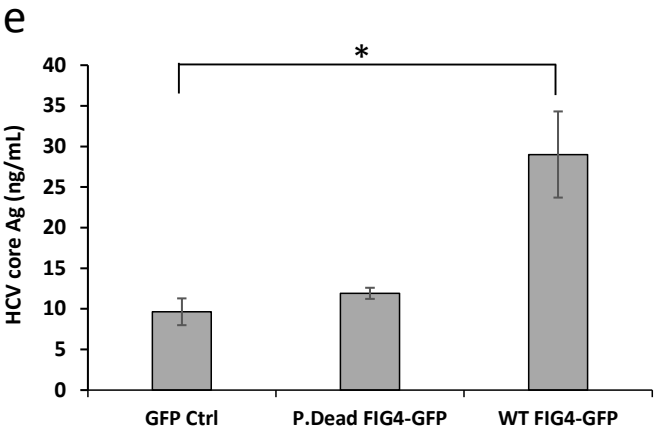

figure
Fig. 6
Click here to download Figure: Figure 6 Cottarel et al..pdf

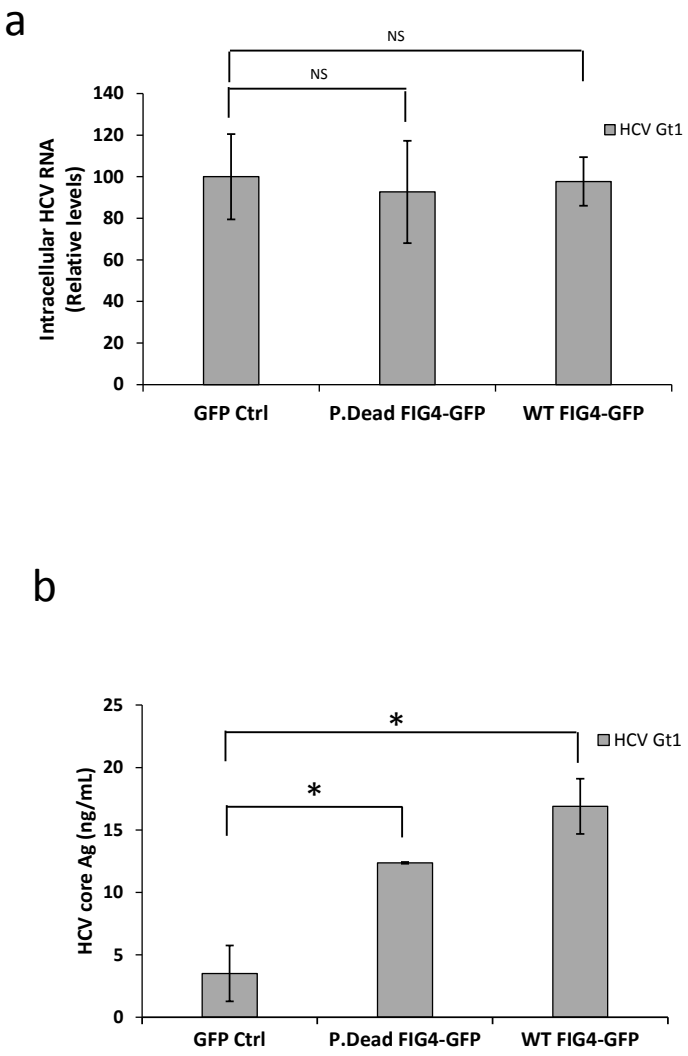

figure

Fig. 7

Click here to download Figure: Figure 7 Cottarel et al..pdf

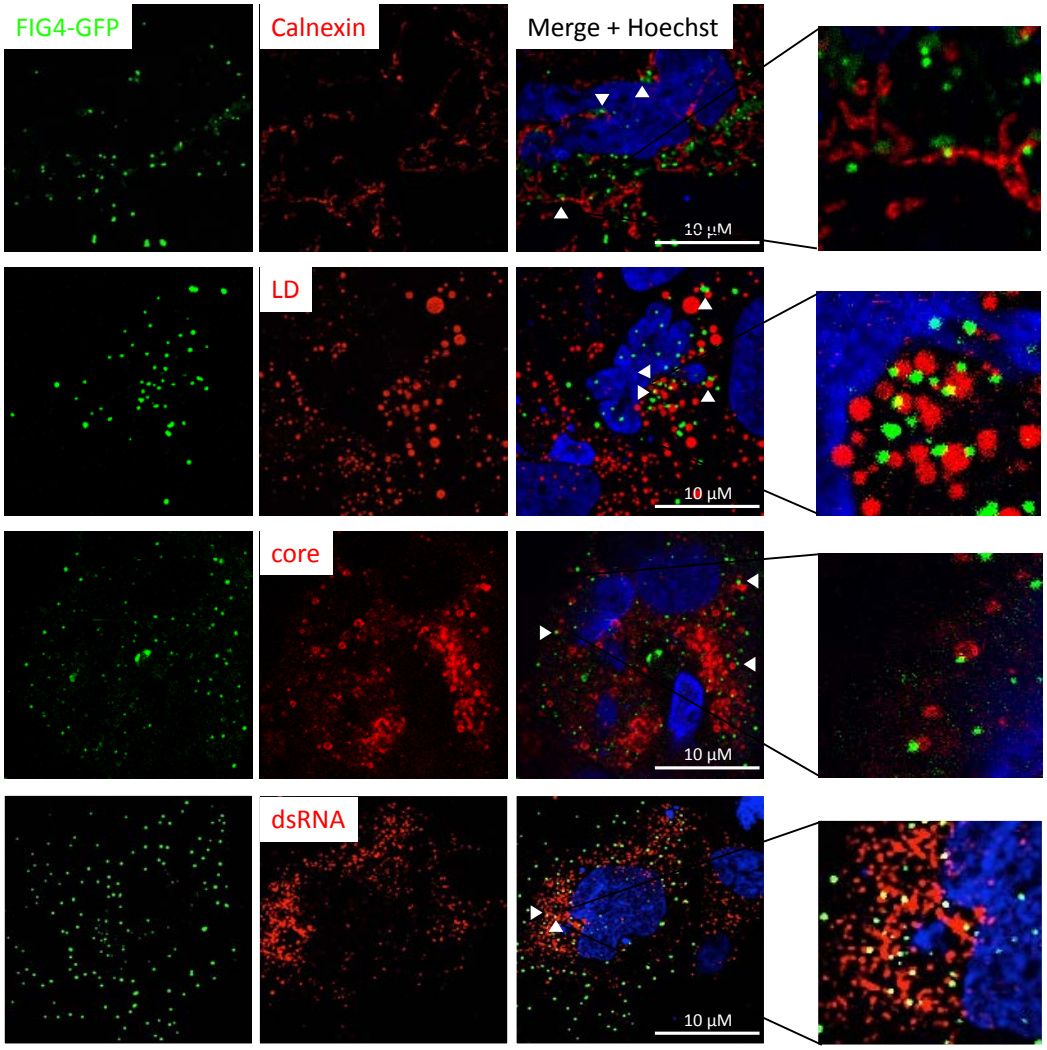

figure
Fig. 8
Click here to download Figure: Figure 8 Cottarel et al..pdf

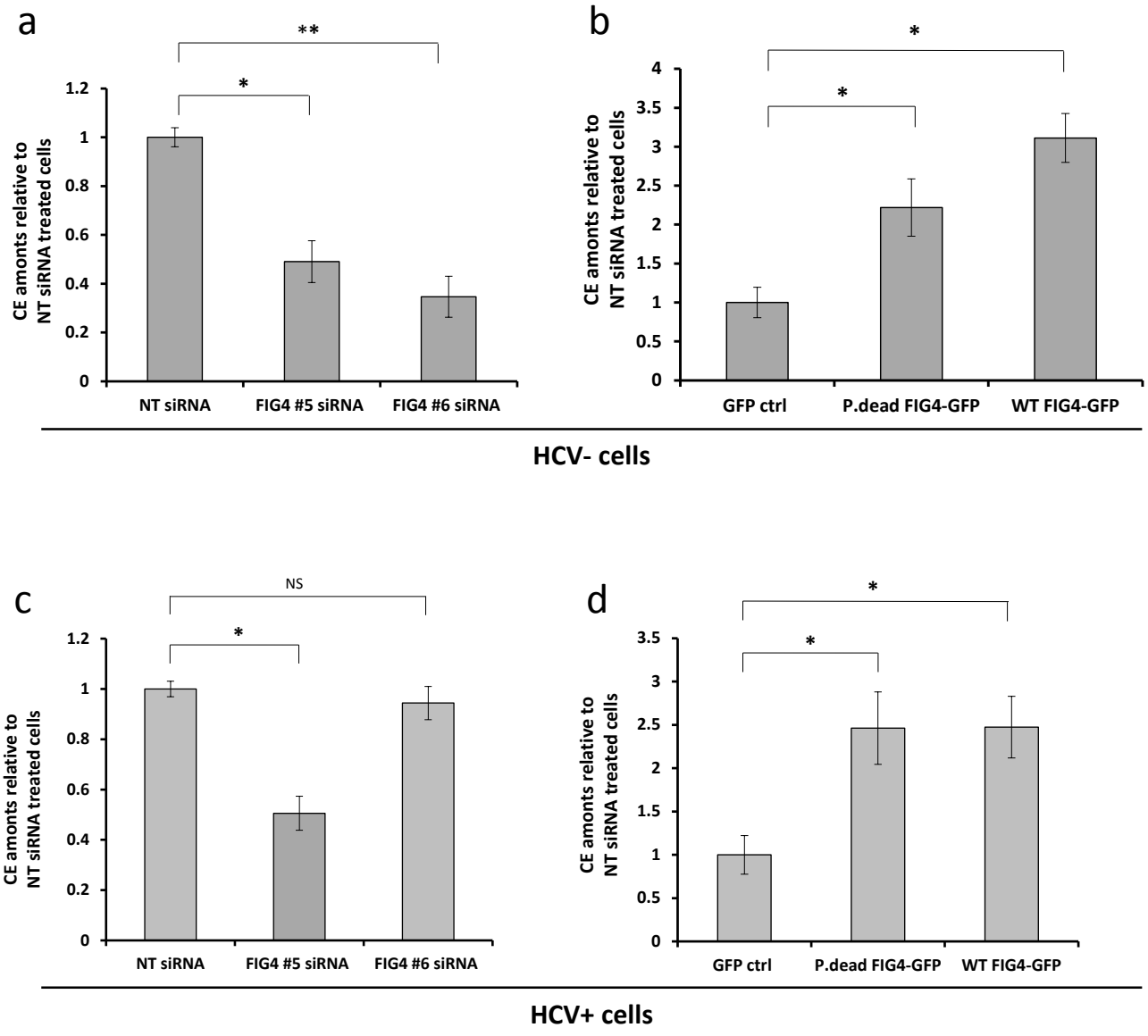

# Supplementary Figure 1

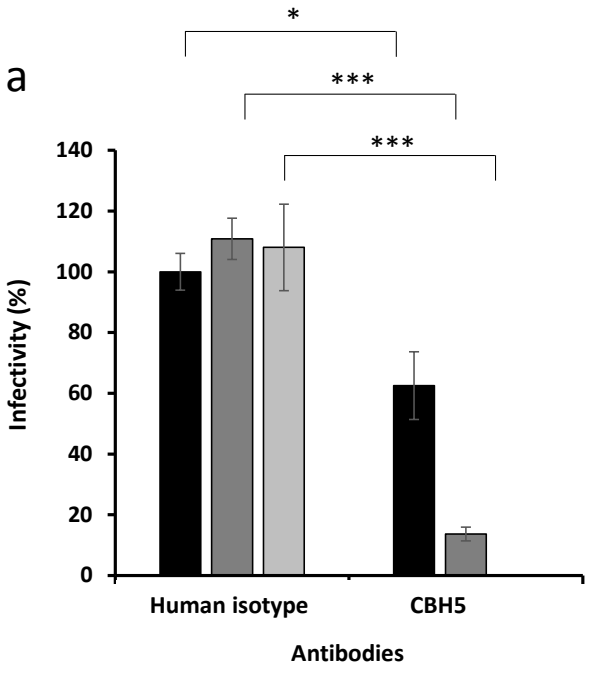


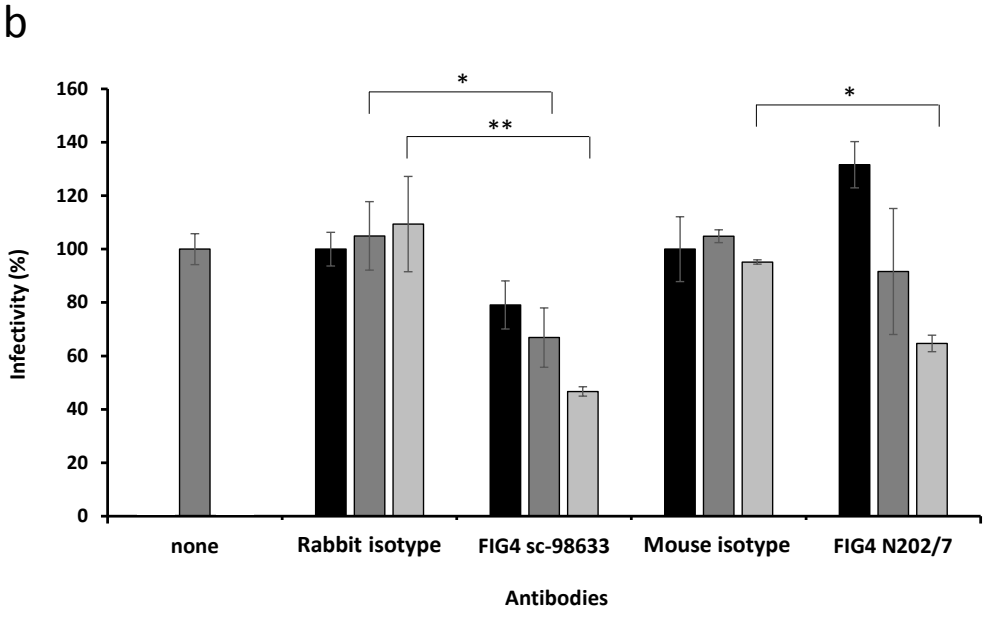

# Supplementary Figure 2

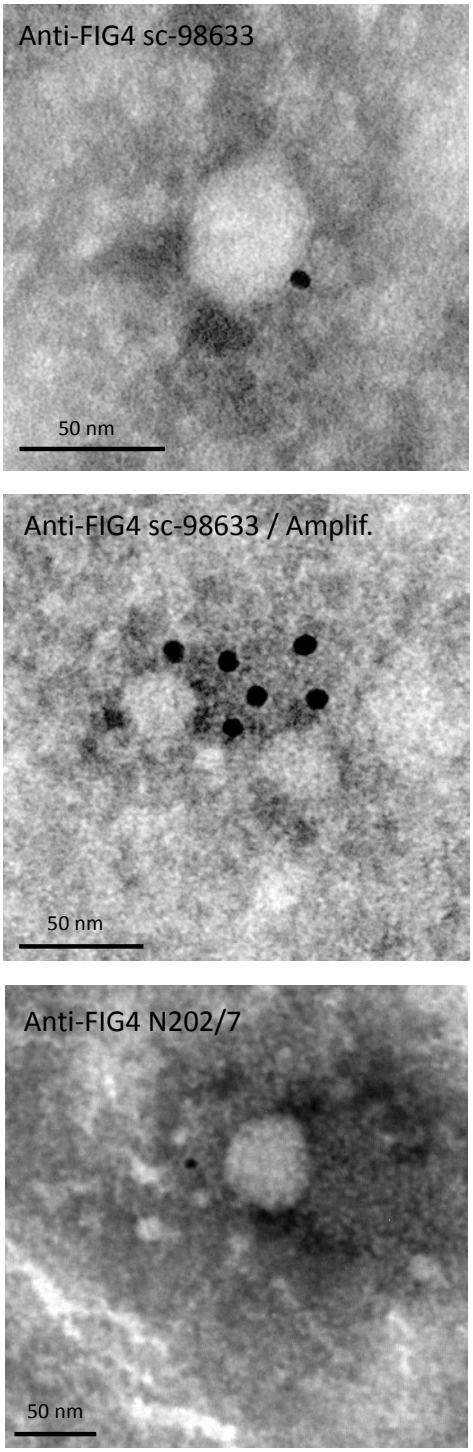

Supplementary Figure 3

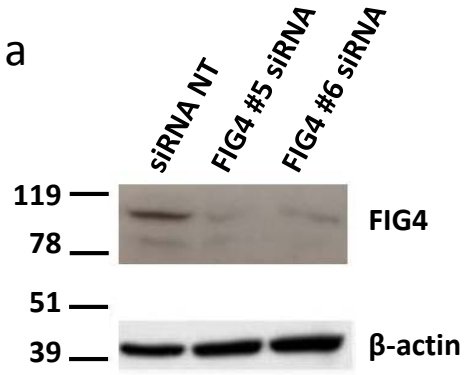


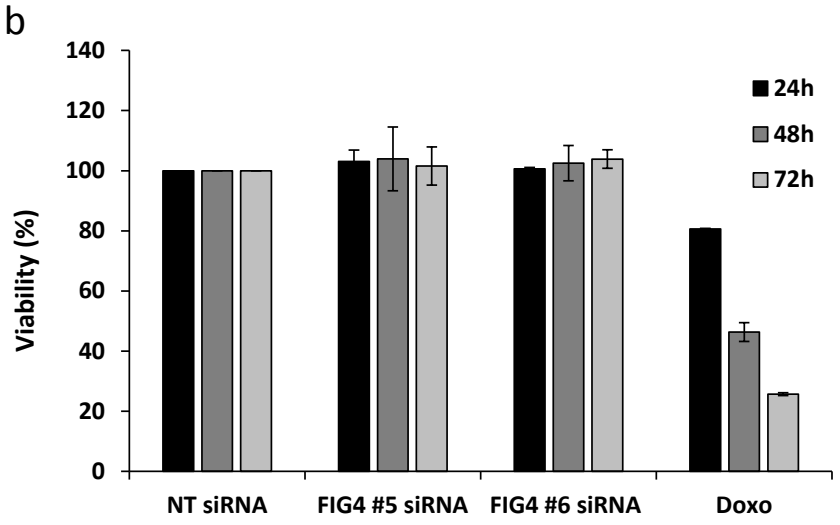


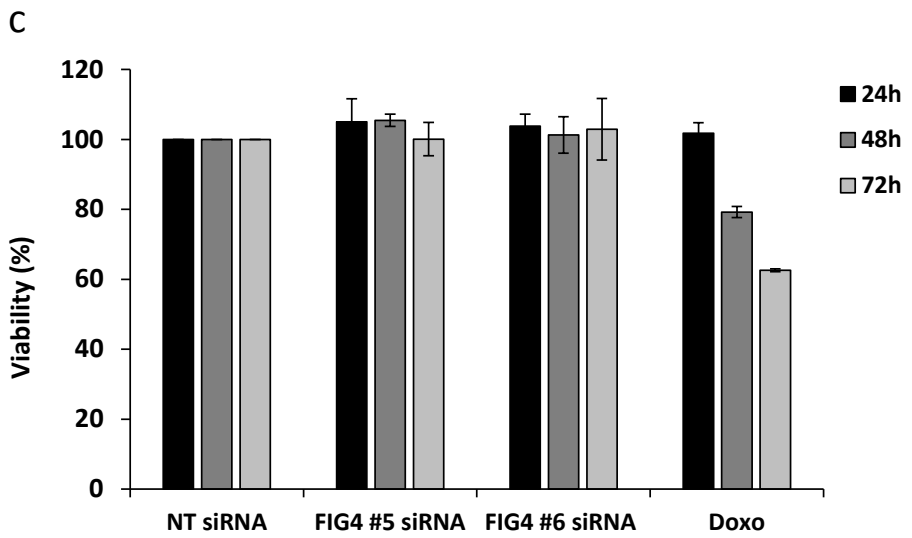

# Supplementary Figure 4

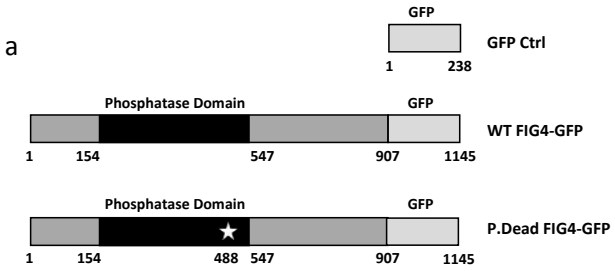


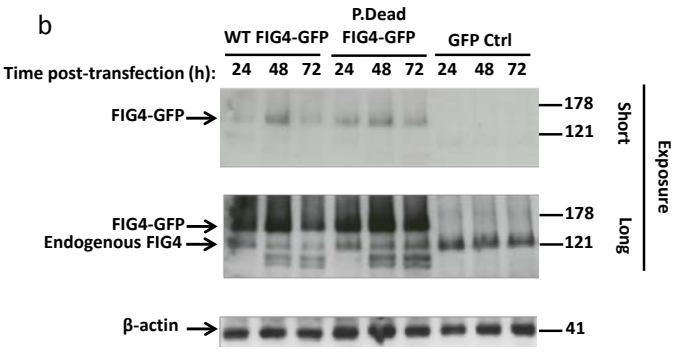


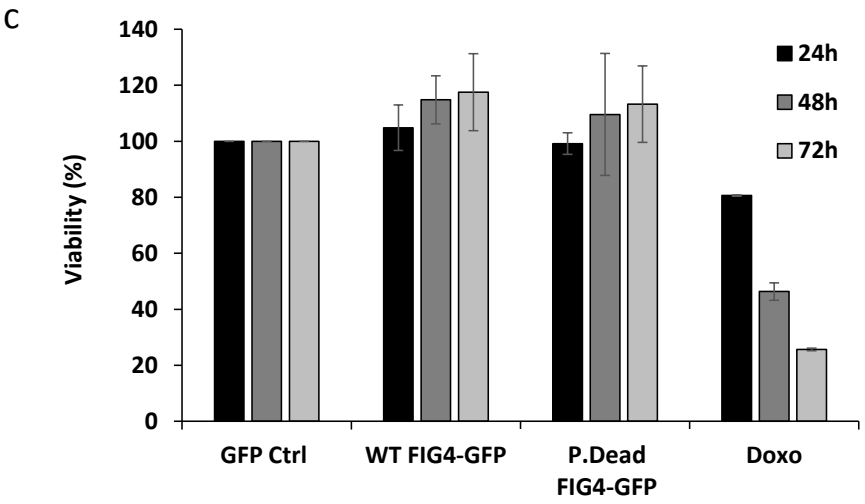


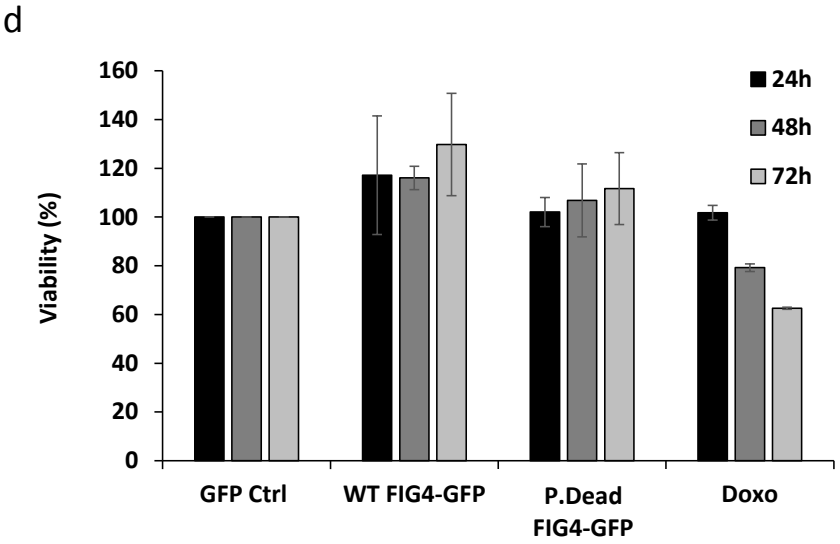

Supplementary Figure 5

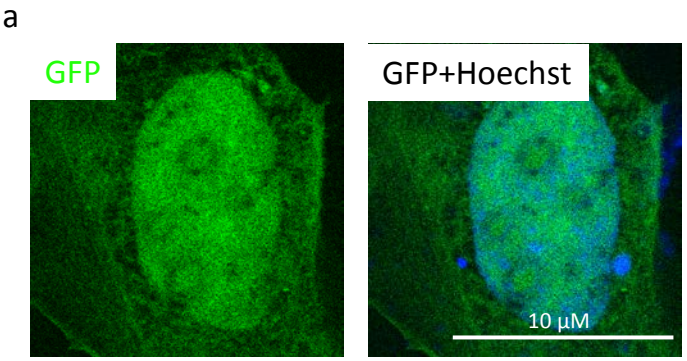


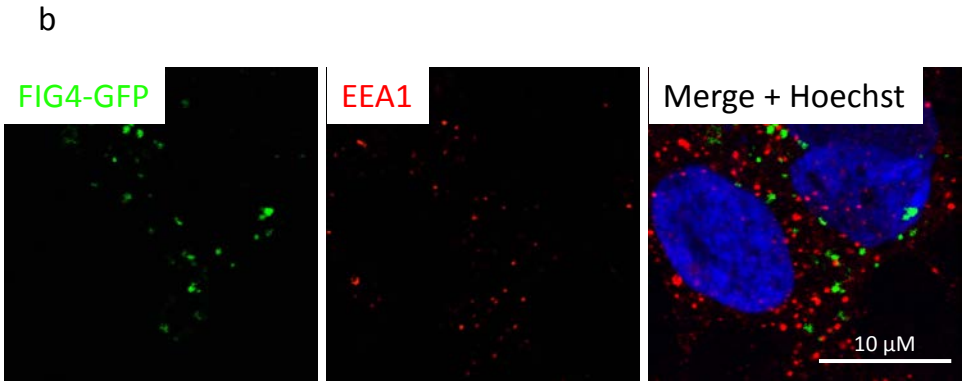

Supplementary Figure 6

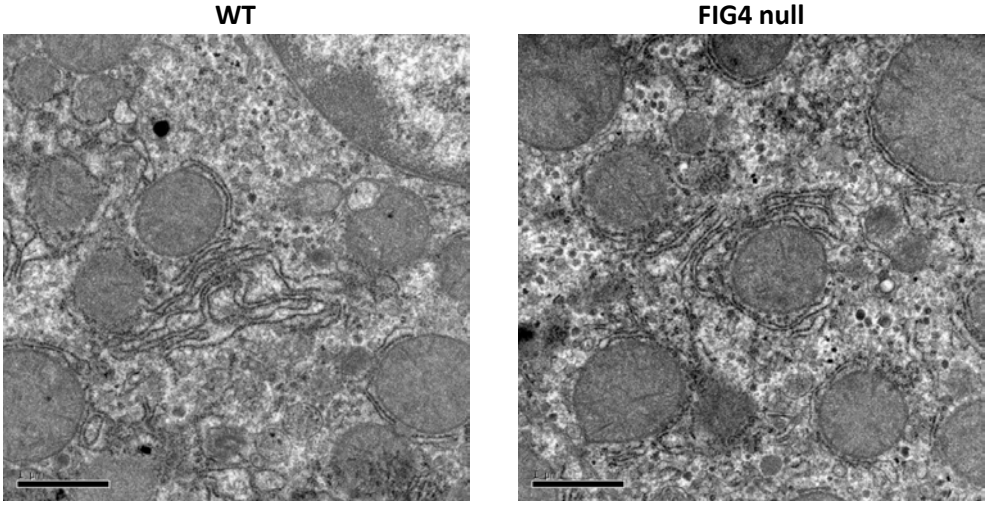

# Supplementary Figure 7

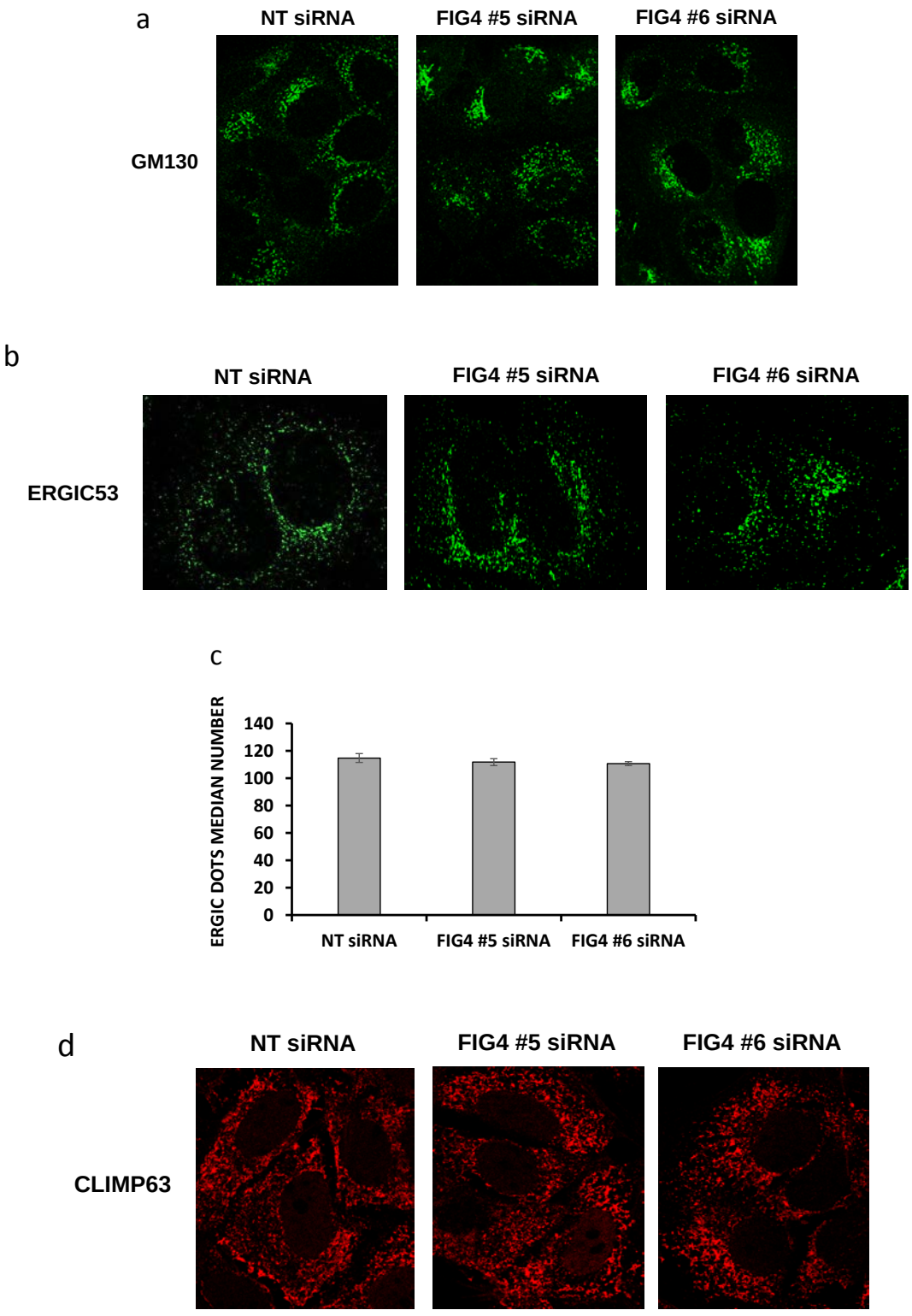

# Supplementary Figure 8

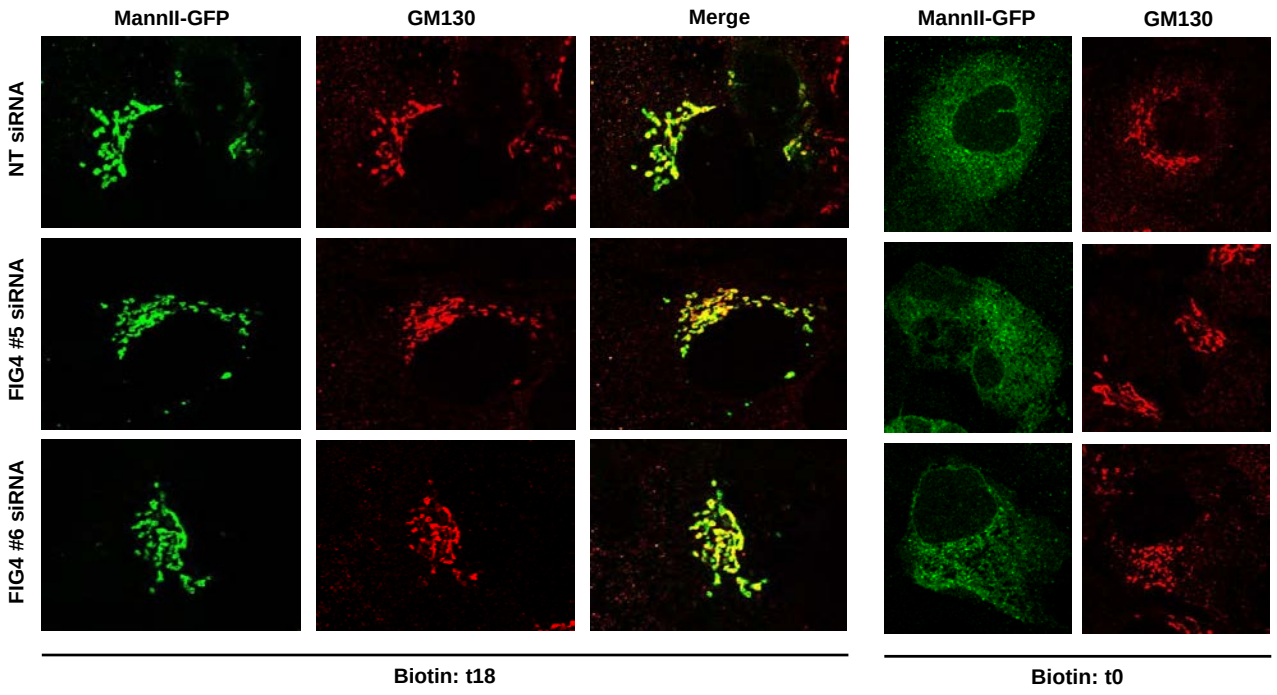

# Supplementary Figure 9

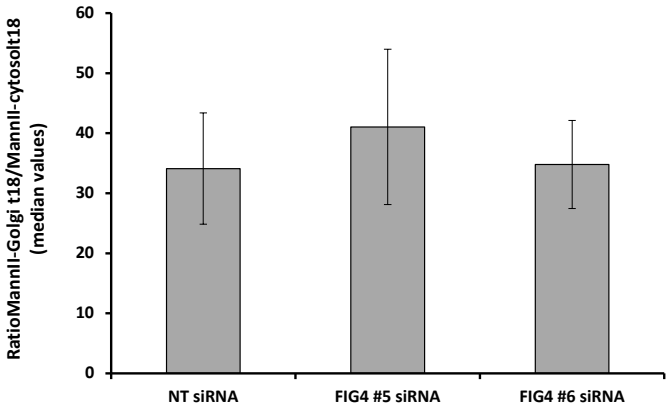

# Supplementary Table 1

| Target name | primers sequences |
|---|---|
| HCV | For GTCTAGCCATGGCGTTAGTA<br>Rev CTCCCGGGGCACTCGCAAGC |
| Gus | For CGTGGTTGGAGAGCTCATTTGGAA<br>Rev TTCCCCAGCACTCTCGTCGGT |
| FIG4 | For ATTCTGTACGGGTTACTCATCCT<br>Rev GCATTCGCAAGACAGTGAGATTA |